Summer 2023

The Future of Alternative Energy? Simulating Methyl Stearate Pyrolysis via Molecular Dynamic Processes

Sarah J. Adeoye
Missouri State University, Adeoye93@MissouriState.edu

THE FUTURE OF ALTERNATIVE ENERGY? SIMULATING METHYL STEARATE PYROLYSIS VIA MOLECULAR DYNAMIC PROCESSES

A Master's Thesis

Presented to

The Graduate College of

Missouri State University

In Partial Fulfillment

Of the Requirements for the Degree

Master of Science, Chemistry

By

Sarah Adeoye

August 2023

THE FUTURE OF ALTERNATIVE ENERGY? SIMULATING METHYL STEARATE PYROLYSIS VIA MOLECULAR DYNAMIC PROCESSED

Chemistry

Missouri State University, August 2023

Master of Science

Sarah Adeoye

ABSTRACT

The process of extracting and refining crude oil is both expensive and environmentally hazardous. The synthesis of biodiesel sourced from vegetable oils is a renewable process and less hazardous to the environment. Therefore, we seek to understand the pyrolysis procedure at an atomic level in hopes of optimizing future fuel viability. Herein, I analyze methyl stearate (a component of biodiesel) using an in-house database of *ab initio* trajectories, each simulating 1.0 ps (with 1.0 fs resolution). These jobs were observed for significant bond-breaking/forming events, the type of fragments produced, and the exact position and time for each event. Statistical analysis was performed on the data to coalesce significant pathways. Programs that employ density functional theory were used to determine their thermodynamic properties with increased accuracy. Understanding the unique characteristics of these fragments is important in engineering future biodiesel formulations as a source of alternative energy.

KEYWORDS: transesterification, methyl esters, density functional theory, molecular dynamics, simulations

THE FUTURE OF ALTERNATIVE ENERGY? SIMULATING METHYL STEARATE PYROLYSIS VIA MOLECULAR DYNAMIC PROCESSES

By

Sarah Adeoye

A Master's Thesis
Submitted to the Graduate College
Of Missouri State University
In Partial Fulfillment of the Requirements
For the Degree of Master of Science, Chemistry

August 2023

Approved:

Matthew R. Siebert, Ph.D., Thesis Committee Chair

Cyren Rico, Ph.D., Committee Member

Richard Biagioni, Ph.D., Committee Member

Keiichi Yoshimatsu, Ph.D., Committee Member

Kevin Evans, Ph.D., Committee Member

Julie Masterson, Ph.D., Dean of the Graduate College

ACKNOWLEDGEMENTS

I would like to express my sincerest gratitude to my supervisor, Dr. Matthew Siebert for his guidance, support, and patience throughout the entire process of conducting this work. His invaluable insights and advice were essential in shaping the direction and focus of my work.

I would also like to thank the past and present Siebert lab members who provided me with encouragement, feedback, and support throughout this journey. Their insights and contributions were truly invaluable and greatly appreciated.

I am also grateful to the staff and faculty at the Department of Chemistry, CNAS, Graduate college and Missouri State University who provided me with access to resources and facilities that were essential to the completion of this study.

I would like to convey my sincere appreciation to God, myself, my family, and friends, particularly my best friend Ashinze Vivian, for their constant support, encouragement, and empathy which kept me determined and inspired throughout this journey.

Thank you all for your contributions, support, and encouragement. Your assistance has been invaluable in making this thesis project a success.

TABLE OF CONTENTS

LIST OF TABLES

LIST OF FIGURES

CHAPTER 1. INTRODUCTION

1.1 Introduction

According to the US Energy Information Administration (EIA), the world has approximately 1.7 trillion barrels of proven oil reserves as of the end of 2021. In terms of the United States, the EIA reports that the average daily petroleum consumption per person was approximately 1.12 gallons, as of 2020, at this current consumption rate, there are approximately 47 years of oil left in the world.[1,2] It is impossible to meet the current energy demand by processing crude oil alone, and the demand is growing exponentially. There is an urgent need to ensure a sustainable supply of energy to meet growing energy demands, one possible form of renewable energy is biodiesel, which is biodegradable, easily available, emits less SOx contamination, emits less soot, is eco-friendly, is non-toxic, and is free of aromatics.[3] According to EIA, fossil fuels, coal, and nuclear fuels, are currently the primary sources of the world's energy supply as illustrated in Figure 1.[4] Despite concerns over natural resource depletion and environmental pollution, renewable energy sources have the potential to address the increasing energy challenges.[4]

Biodiesel is composed of fatty-acid methyl esters (FAMEs), which come from fats and oils found in nature.[5–26] These FAMEs are distinguished by the presence of monoalkyl chains ranging in length from 12 to 20 carbons. Soybean is the most common source of biodiesel in the United States and canola (rapeseed oil) in Europe.[27,28]

1.2 Criteria for Selection of Alternative Energy

The major drawback to the use of fossil fuels as a source of energy is their adverse effect

on the environment through the emission of CO_2, NOx, and soot particles. Biodiesel production currently costs 1.5 times more than petroleum production from fossil fuels because of the high cost of using vegetable oil as a source of raw material.[29–32] To combat the high cost of biodiesel production, computer simulations are being employed to help optimize the process. Petroleum and natural gas have a very high utilization rate of 35% and 34% respectively compared to other sources (Figure 1). Sustainable energy sources that do not rely on fossil fuels and have minimal adverse impacts on the environment must be developed to meet rising global energy demands.

Even though it is difficult to find an alternative source of energy that considers all other fossil-fuel-generated commodity products, it is of the utmost importance from a moral standpoint to steer society away from "solutions" wrought with problems that will have to be resolved in the future. In the quest for other energy forms, some guiding principles to consider are: [34–37]

1. High Efficiency: Refers to the amount of practical energy that can be derived from a specific energy source.
2. Renewability: Energy sources should be renewable and capable of being replenished over time.
3. Environmental impact: The energy source should cause little to no pollution and have minimal negative effects on ecosystems, for example, through the release of CO_2, NOx, and soot particles.
4. Cost: Energy sources should be cost-effective and economically viable.
5. Scalability: The energy source should be able to meet society's exponentially increasing energy demands.
6. Social acceptance: The energy source should be accepted by the public.

From these criteria stated above, even fossil fuels, coal, and natural gas are less than optimal owing to rates efficiency due to the large amount of energy lost during the combustion process.[38] The energy source being explored should have the capacity to be replenished on a human timescale, which presents a limitation on nuclear power. Additionally, uranium, which is used to power nuclear plants, is limited in supply and very expensive to procure. The faster we can regenerate an energy source, the more easily replenished it is.

1.3 Biodiesel as a Suitable Replacement to Petroleum

Apart from its use as a transport fuel, there are other uses of fossil fuels including the production of fertilizers and pesticides for farming, cosmetics and personal care products, lubricants, synthetic rubber, antibiotics, heating oils, waxes for pharmaceuticals, and chemicals for industrial uses. [39–41] It is imperative to find an alternative source for these needs as well, pyrolysis of biodiesel holds promise in this regard.[36] Concerted efforts are being made to explore other sources of energy, it would be convenient for these alternative energy sources being considered to have the same physical, and thermochemical properties as conventional crude oil and be as carbon neutral as possible.[42] Unlike biodiesel, the processing of petroleum-derived diesel is costly and has adverse effects on the environment due to the exploratory, drilling, refining, and transport activities involved in its production. [5,43,44]

Conventional biodiesel has its own limitations as a fuel source, including inoperability in cold climates due to a low pour point of -9 to 15 °C, economically costlier to process than conventional crude oil due to the complexity of biodiesel components, and dislodging of engine deposits.[37,45] Mathematical optimization models can be used to combat the issue of high cost of production, these models can determine supply chain design while also taking into account

supply chain configurations, production locations, biomass supply, transport, and storage modes.[46] Using low feedstock materials such as waste cooking oil, animal fats can also significantly reduce the cost of production.[17,47] To reduce inoperability in cold climates and alleviate dislodging of engine deposits, biodiesel can be heated prior to use, and blended with additives such as antioxidants, cetane enhancers, cold flow improvers, and other fuels. Another method is to subject biodiesel to a process known as winterization, in which high melting saturated esters are ejected by repeating cooling cycles.[18] Provided that the limitations of biodiesel as an energy source are duly acknowledged and appropriate actions are taken to mitigate them, biodiesel continues to represent a viable and promising alternative to petroleum.

1.4 Transesterification Reaction of Triglyceride Feedstocks

The synthesis of biodiesel involves the transesterification of triglycerides with an alcohol in the presence of a catalyst to produce long-chain mono-alkyl esters and release glycerol; a commodity product as shown in Figure 2.[5,7,8,10–26,48] If methanol is used to produce biodiesel, the product of the transesterification reaction is known as fatty acid methyl ester (FAME); if ethanol is used, it is known as fatty acid ethyl ester (FAEE); and if propanol is used, it is known as fatty acid propyl ester (FAPE). The type of FAMEs produced is determined by the triglyceride feedstock used. [49]

1.5 Classification of Commonly Found FAME in Biodiesel

Subsequently, fatty acid methyl esters (FAMEs), which are components of biodiesel, are thermally cracked to produce lightweight hydrocarbons or transport fuels, such as natural gas, kerosene, and gasoline. The most common types of FAMEs found in biodiesel are methyl oleate,

$C_{19}H_{36}O_2$ (C18:1) where 18 represents the number of carbon bond, and 1 represents the number of unsaturation), methyl palmitate $C_{17}H_{34}O_2$ (C16:0), methyl stearate $C_{19}H_{38}O_2$(C18:0), methyl linoleate $C_{19}H_{34}O_2$ (C18:2), methyl and linolenate $C_{19}H_{32}O_2$ (C18:3) as shown in Table 1, which are a combination of saturated and unsaturated chains; their structures are shown in Figure 3, the degree of unsaturation of these FAMEs influences the characteristics of biodiesel.[50]

Some studies have shown that an increase in the degree of unsaturation (iodine number) can increase the emission of NO_x, and thermal NO_x can be produced by biodiesel fuels with higher unsaturation. Even fossil fuels, coal, and natural gas are less than optimal owing to rates efficiency due to the large amount of energy lost during the combustion process.[51]

This is because the combustion process of biodiesel with higher unsaturation produces carbonized high-temperature areas, the number of double bonds reduces the length of the chain, which then reduces the cetane number; allowing for better mixing of air and water, which then leads to better combustion and lesser NO_x emissions, while for the saturated ones, the NOx emissions increased with reducing chain length.[51] This is not a direct comparison, as some FAMEs have shown a reverse relationship depending on the feedstock used. This makes the relationship between NO_x and saturation of FAMEs a complex one.[52–55] Depending on the feedstock utilized, the FAME content of biodiesel also changes. Soybean oil, rapeseed oil, palm oil, and animal fats are the common feedstocks used to produce biodiesel. Saturated FAMEs such as methyl palmitate (C16:0) and methyl stearate (C18:0) are those commonly found in animal fats.[28,56]

1.6 Why Methyl Stearate as a Choice of FAME for This Study is Better

Methyl Stearate was chosen as the basis for this study due to its fully saturated alkyl

chains, as opposed to unsaturated methyl esters methyl linoleate, linolenate, and oleate. The saturated chain portions of these methyl esters are resistant to decomposition; they have lower reactivity at reduced temperatures than their unsaturated counterparts because of the absence of double bond moieties in their structure. The allylic carbon in unsaturated FAMEs is very reactive, and the hydrogen on that carbon can be easily abstracted, leading to a chain of reactions. The presence of a high percentage of saturated FAMEs can provide biodiesel with excellent oxidation resistance but also cause gelling of fuel in colder climates, while the low melting point of unsaturated FAMEs makes them more useful for biodiesel production but makes them prone to oxidation and rancidification.[58] Overall, the inclusion of methyl stearate as a component in biodiesel can improve the oxidative stability of the fuel and provide better resistance to decomposition, as compared to its unsaturated counterparts. Its fully saturated alkyl chain structure results in lower reactivity at reduced temperatures, making it a valuable addition to biodiesel fuel formulations.

1.7 Pyrolysis of Methyl Stearate

To bridge the gap between the heavy reliance on petroleum-derived diesel and other alternative energy sources, this study focuses on the pyrolysis of FAMEs, which involves the thermal decomposition of long-chain hydrocarbons into low- to medium-weight hydrocarbons in the form of gases, organic liquid products (OLP) and tar (solids) that are similar to petroleum and can be subsequently used for different industrial purposes. This process involves the exposure of long-chain hydrocarbons to high temperature and pressure in an anaerobic environment, which results in successive and simultaneous reactions, making pyrolysis a very complex process. The resulting commodity chemicals can then be extracted using fractional

distillation and distributed for various applications.[5,37,59–62]

Table 1. Average FAME composition (wt.%) of Soybean oil, rapeseed oil, and sunflower oil issued from plants[57]

Type of FAME	Soybean	Rapeseed	Palm oil
Methyl Stearate (C18:0)	4	2	4
Methyl Oleate (C18:1)	23	62	41
Methyl Palmitate (C16:0)	12	4	43
Methyl Linoleate (C18:2)	54	22	10
Methyl Linolenate (C18:3)	6	10	0

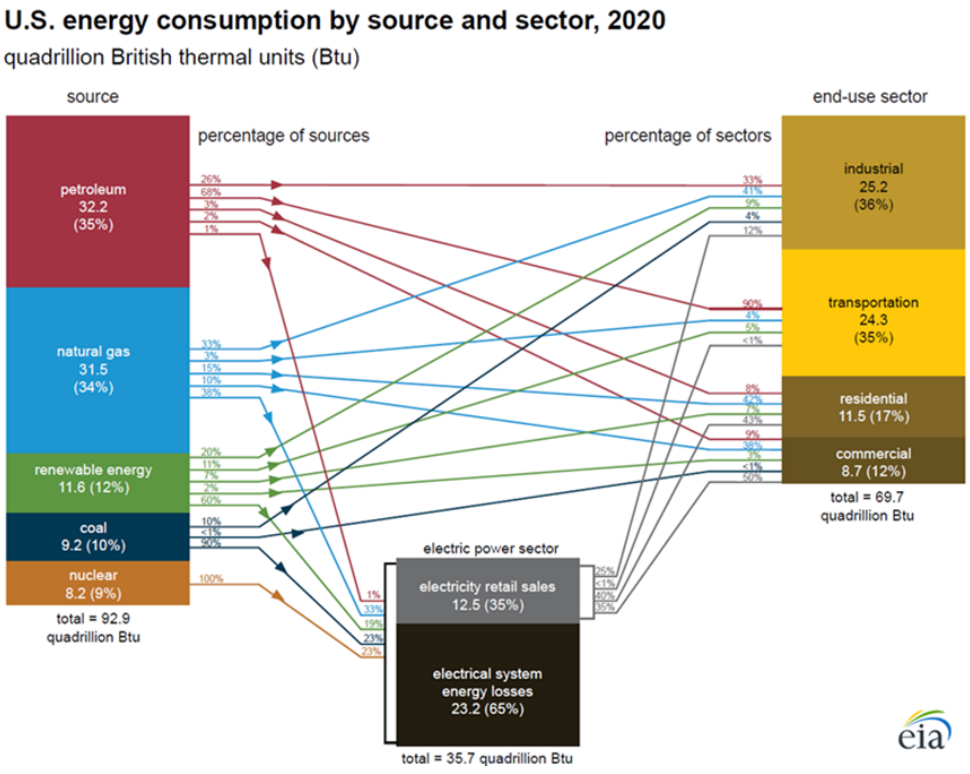

Figure 1. Energy diagram showing energy utilization rate and sources for the United States in 2021[33]

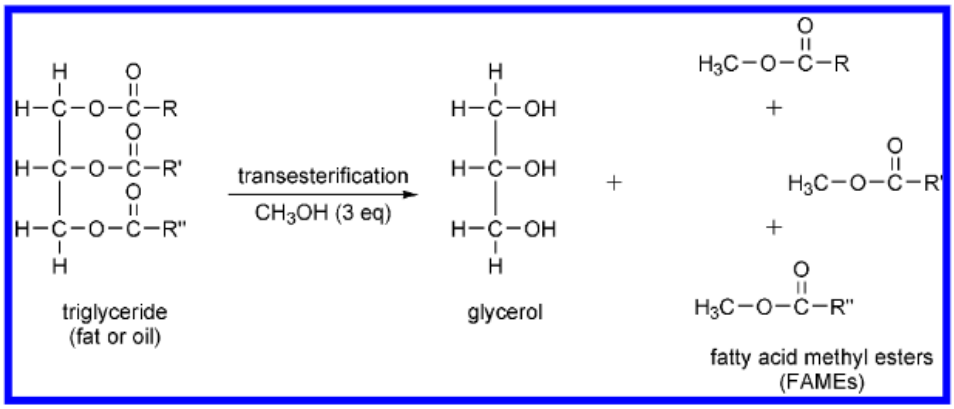

Figure 2. Transesterification of a triglyceride in the presence of methanol to give FAMEs[5]

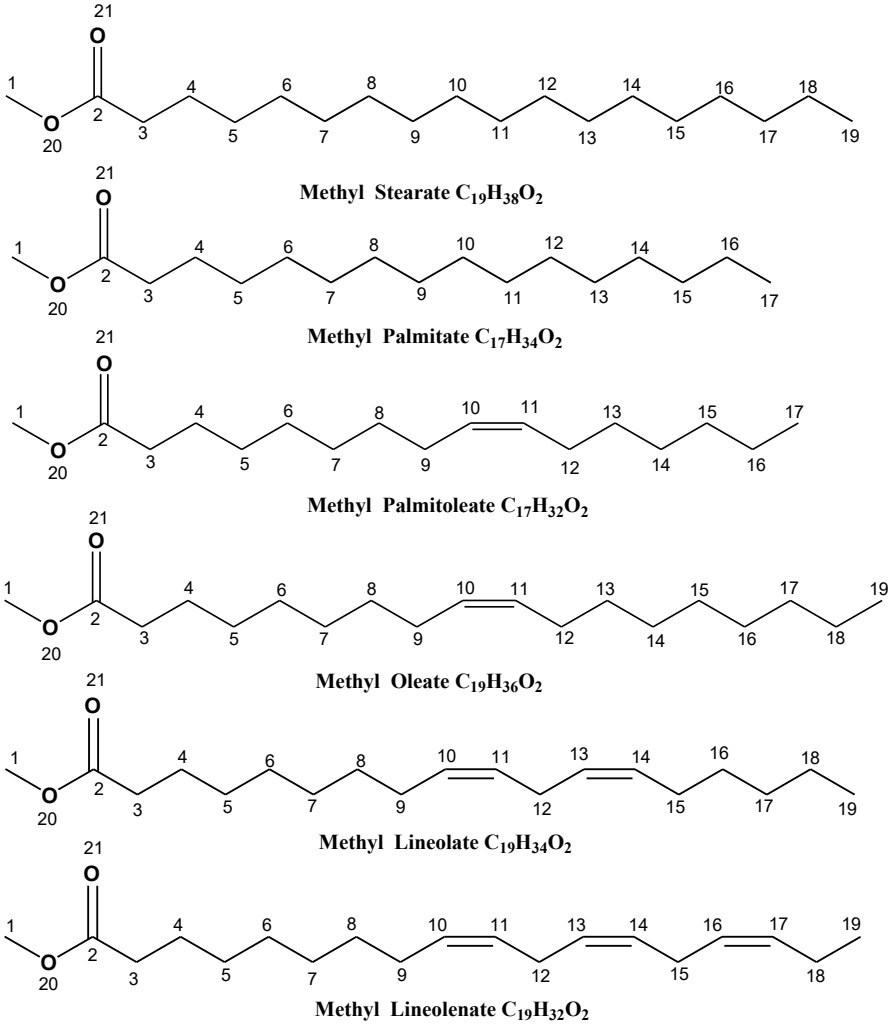

Figure 3. Structure of commonly found FAMEs in Soybean

CHAPTER 2. MODEL AND METHODOLOGY

2.1 Density Functional Theory

Electronic structure theory employs fundamental physical principles as a framework to investigate the electronic structure and properties of atoms, molecules, and solid-state materials. Density functional theory is a quantum mechanical method that uses the electron density of a system as the fundamental variable, rather than the wave function that is familiar to elementary quantum chemistry studies. Traditional electronic structure methods which use wavefunction Ψ as the central quantity have been widely used to describe the behavior of atoms and molecules by using the many-body wave function to describe the behavior of N interacting electrons in an external electrostatic potential, which becomes difficult with increasing N, and increases computational cost to describe larger systems. The wave function depends on 4N variables, three spatial and one spin variable for each of the N electrons, which becomes unmanageable for large systems like proteins and triglycerides. Density-functional theory provides a powerful alternative to traditional electronic structure calculations for the description of large systems by using the one-body density as the fundamental variable.

In density functional theory, the total energy of a system is expressed as a function of the electron density, and the electron density is determined by solving the Hohenberg-Kohn and Kohn-Sham equations, which are a set of relativistic or spin-dependent Schrodinger-like equations. The fundamental equation of DFT is the Hohenberg-Kohn theorem, which states that the external potential and electron-electron interactions uniquely determine the ground-state electron density of a many-electron system. The Kohn-Sham equation, which is a set of non-interacting, effective single-particle equations that produce the same electron density as the true

many-electron system. These equations yield the electronic wave functions and energies, which can be used to calculate various system properties, such as the total energy, electron density, and potential energy. The Hamiltonian operator of a system is defined by N, the number of electrons R_A, the position of the nuclei in space, and Z_A the charges of the nuclei. $\rho(r)$, electron density which determines the probability of finding any of the N electrons within the volume element of the ith electron $d(r_i)$ but with arbitrary spin while the other N-1 electrons have arbitrary spins and positions represented by Ψ. $\rho(r)$ goes to infinity and integrates to the total number of electrons as expressed below.[63]

$$\int \rho(r \to \infty) = 0 \tag{1}$$

$$\int \rho(r_i)\, dr_i = N \tag{2}$$

$$\lim_{r_{iA} \to 0} \left[\frac{\partial}{\partial r} + 2\, Z_A\right] \bar{\rho}(r) = 0 \tag{3}$$

i.e., density at the position of the nucleus contains information about the nuclear charge Z. Thus, the electron density provides all the information for setting up the operator.[63] The operator of the system in a ground-state DFT calculation is expressed as:

$$\hat{O} = \hat{T} + \hat{U} + \hat{V} \tag{4}$$

where T is the kinetic energy, U is the electron interaction energy, V is the potential energy from the external field due to positively charged nuclei. The ground-state energy E_0 can be written as a functional of the density $E_{v_0}[n]$, which gives the ground state energy E_0 if and only if the true ground-state density $n_0(r)$ is inserted. For all other densities $n_0(r)$, the inequality

$$E_0 = E_{v_0}[n_0] < E_{v_0}[n] \quad (5)$$

holds.[64]

For a given system particle-particle interaction $F[n]$ is a universal that is independent of the potential $v_0(r)$ of the system under consideration.[64]

$$F[n] \equiv (T_s[n] + U[n]) + E_{xc}[n] \quad (6)$$

Thus, the energy functional for a given potential $v(r)$, energy functional is,

$$E_{v_0}[n] = F[n] + \int d^3r v_0(r) n(r) \quad (7)$$

Hohenberg and Kohn then established that the density functional attain the minimum (from above) for the correct state density $n(r)$ provided the total number of particles is kept constant.[65]

$$N[n] \equiv \int n(r) dr = N \quad (8)$$

Following that, it was demonstrated that density $n'(r)$ in relation to another potential $v_0'(r)$, that differ from $v_0(r)$, leads to a minimum value of the energy functional that is greater than the ground state density $n(r)$ of the system, establishing the following inequality,[64,65]

$$\int d^3r v_0(r) n'(r) + F[n'] > \int d^3r v_0(r) n(r) + F[n] \quad (9)$$

This inequality expression is referred to as the second Hohenberg and Kohn theorem or as the DFT variational principle.[66] DFTs widespread applicability can be related to its balance between computational cost, accuracy, and precision. One major setback with utilizing the DFT methods is the complexity of the exchange-correlation functional approximation, which determines the accuracy of a given DFT method. This functional must be integrated by setting a grid size. Density functional approximations are generally unreliable for anions, charge transfer systems, and point defects. They cannot accurately describe dispersion forces, which are essential when studying noncovalent reactions involving large molecules. By utilizing small double-basis sets, such as 6-31G, we can reduce the computational cost of dispersion-corrected DFT, thereby enabling the modeling of large molecular systems.

Functional and basis sets are essential components of a theoretical calculation in computational chemistry.[66] A basis set is a set of mathematical functions that is used to represent the electronic wave functions as a linear combination of basis functions; these are usually atomic orbitals of the atoms approximated as Gaussian function. Computation cost grows rapidly with increasing size of the basis set, so a compromise needs to be made between accuracy and cost when deciding on a basis set. In contrast, the functional is a mathematical expression that describes the relationship between the electron density and the system's total energy.

In DFT, the electronic wave function is replaced by the electron density, and the functional is applied to the electron density to calculate the total energy of the system. Different functionals have varying degrees of precision and computational efficiency, and the choice of functional depends on the system being studied and the desired degree of precision. The choice of basis set and functional can have a substantial effect on the accuracy and efficiency of a calculation, and both must be selected with care based on the system being studied and the

desired level of accuracy. M06-2X, which is a highly parametrized exchange-correlation energy functional that is very accurate in describing the thermochemistry of main group elements, was chosen based on the studies carried out in order to determine the better functional between B3LYP/6-31+G (d, p) and M06-2X/6-31+G (d, p) based on the prediction of bond dissociation energy of 44 chemical moiety representative (CMR) reactions. The M06-2X/6-31+G (d, p) functional outperformed the B3LYP functional.[5,37,67]

2.2 Local Density Approximation

The local density approximation (LDA) functional is the simplest exchange functional. The LDA exchange functional assumes that the exchange energy density at every point in space for an atom or molecule may be described as the exchange energy density of the homogenous electron gas (HEG) model with the same density, i.e., exchange correlation energy is purely local. It is a simpler and computationally cheaper alternative to more accurate but more sophisticated methods such as full configuration interaction (FCI) and configuration interaction (CI). For a spin-unpolarized system, the LDA approximation for exchange-correlation energy is[68]

$$E_{XC}^{LDA}[p_0] = \int [p_0](r)\varepsilon_{XC}(r)d(r) \qquad (10)$$

where $[p_0](r)$ is electron density at point r and $\varepsilon_{XC}(r)$ is the exchange correlation energy per particle of a HEG gas.

Equation 10 decomposed into a linear relationship between exchange and correlation terms.

$$E_{XC} = E_X + E_C \quad (11)$$

2.3 Computer Modelling

Little to no knowledge is known about the thermal decomposition of FAMEs, and there is insufficient data to validate their kinetic models because of the complexity of the feedstock used. However, reactions in pyrolysis processes are believed to occur with rapid free-radical initiation at very high temperatures, which are difficult to detect and replicate experimentally. Computational investigations were performed to better understand the thermal cracking of FAMEs. Because the experimental pyrolysis of FAMEs is more expensive than the processing of petroleum-based fuels, there is a need to investigate a cheaper alternative. Computer simulations of the pyrolysis process provide a cost-effective option for observing and understanding the thermochemical properties of pyrolysis. Quantum mechanical (QM) calculations are based on the principles of quantum mechanics and can describe the behavior of electrons and nuclei in a molecule. Quantum mechanical calculation can offer precise transition states and reaction rate constants.[69]

Trajectories of pyrolysis of FAME can be generated from quantum mechanical (QM) calculations using the methods of molecular dynamics (MD) simulations. In this approach, the potential energy surface (PES) of the system is calculated using QM calculations, which describe the electronic structure and energetics of the system. The PES is then used to generate a set of initial conditions for the MD simulation, which includes the positions and velocities of the atoms and molecules in the system. The simulation is then run, and the motion of the atoms and molecules is tracked over time to generate a trajectory. Several trajectories are generated to

obtain statistically significant results and to capture the variability of the pyrolysis process since a single run cannot provide enough mechanistic information on the thermodynamic properties of the pyrolysis processes. These simulations can provide useful insight into the complexities of the pyrolysis process and aid in the development of methods for producing higher-quality biofuels while also increasing efficiency.

2.4 Processes Involved in an MD Simulation

In a molecular dynamics (MD) simulation of pyrolysis, an ensemble of FAME molecules at a defined temperature and pressure is used as the initial state. The simulation employs Newton's equations of motion to track the movement of atoms and molecules in response to intermolecular forces. The simulation advances in 1 fs time increments, and at each step, the atoms' positions, velocities, and other characteristics are updated based on the acting forces. This process is repeated until the simulation's end point or until the pyrolysis reaction is complete. To replicate the heating phase of the pyrolysis reaction, the system's temperature is gradually increased during the simulation. As a result, the atomic and molecular bonds vibrate and eventually break, leading to the formation of new substances. The pyrolysis reaction's kinetics are analyzed, documented, and compared to experimental data to assess the simulation's validity and enhance its parameters.

The simulation of pyrolysis of FAMEs can be computationally intensive, expensive, and difficult to execute. There needs to be a balance between computational cost and effectiveness. Numerous computer modeling methods have been employed to simulate the pyrolysis of FAMEs, such as Bond Dissociation, Ab initio methods, and Reactive force field (ReaxFF). In this work, we explored the advantages and limitations of each of these approaches.

2.5 Bond Dissociation Modelling

Dissociation of a bond is caused by the vibration of the atoms about that bond, bond dissociation modeling uses the energy (B.D.E) required to break a bond as a measure of the reaction rate. A bond will break when the vibrational energy is greater than the bond dissociation energy (B.D.E).[70] Thus, radical formation, reaction rates of pyrolysis of FAMEs, and product distribution can be predicted with B.D.E. Radicals play a crucial role in determining the mechanism of a reaction. Optimal processing conditions like temperature, pressure, and residence time can be determined to produce high yields of products. Due to the complexity of the reaction pathways involved in a pyrolysis reaction, there is a likelihood of incorrect predictions of reaction rates.

FAMEs can undergo pyrolysis via multiple reaction mechanisms, including homolysis, heterolysis, and the radical reaction. Bond dissociation modeling works on the assumption that these reactions proceed at a constant temperature, which is not the case for a pyrolysis reaction as the temperature fluctuates based on the time and location in the reactor, thereby affecting the reaction kinetics. It is difficult for bond dissociation modeling to accurately predict these reactions based on these observations.

2.6 Ab-initio Methods

These methods predict the properties of a system by solving the electronic structure of a molecule using charges, masses of electrons, and nuclei without the use of any experimental data or previously determined empirical data. Ab-initio methods have proven to show very high consistency with experimental data. To achieve this level of accuracy, they require a very high computational cost and effort.[71] They can be applied to a wide range of systems, from small

molecules to macromolecules. Ab-initio methods can be computationally expensive for very large systems that require high accuracy and might not be suitable for systems or reactions that involve large energy barriers or systems with highly correlated electronic states.

2.7 Reactive Force Field

Reactive Force Field, or ReaxFF, on the other hand, calculates the forces between atoms and molecules in a system by employing a combination of classical and quantum physics with minimal computational effort. It incorporates van der Waals coulombic interactions at each time step of the simulation. It considers the electronic structure of atoms and molecules, as well as bond-breaking and forming processes that occur during a chemical reaction.[69,72] ReaxFF is usually used to predict large, complex systems like the pyrolysis of biodiesel and can be more computationally efficient than the ab-initio method. The accuracy of ReaxFF is highly dependent on the quality of the force field parameters used, which are usually obtained by fitting to experimental or ab initio data. This can limit the generalizability of ReaxFF to systems that are significantly different from those used in the parameterization process. To ensure the accuracy of the results, ReaxFF simulations must be carefully validated against experimental data or higher-level theoretical calculations. The total potential energy of a system is given by:

$$E_{system} = E_{bond} + E_{over} + E_{under} + E_{val} + E_{pen} + E_{tors} + E_{conj} + E_{vdwaals} + E_{coulomb} \quad (12)$$

Where E_{system} is the potential energy of the system, E_{bond} is the bond energy due to interatomic distances between a pair of atoms, E_{over} is the over-coordinated atom in the energy contribution,

E_{under} is the under-coordinated tom in the energy contribution, E_{val} is the valence angle term, E_{pen} is the penalty energy, E_{tors} is the torsion energy, E_{conj} is the conjugation effect to molecular energy, $E_{vdwaals}$ is the non-bonded Vander Waals interaction, and $E_{coulomb}$ is the coulombic interaction.

2.8 Energy Calculations for Molecules of Methyl Stearate

The energy calculations for a system involve the total energy of that system, which includes the bond energy between atoms, the energy of the system, and the energy of the electron distribution. Calculation of the fixed geometries of nuclei is important in molecular dynamics. There are two commonly used methods used to make these calculations, which are molecular dynamics and density functional theory. On the other hand, electronic structure methods are usually more computationally expensive for very large systems like proteins and biodiesels than small systems due to the increased complexity and number of atoms involved. The methods used for these energy calculations differ in their treatment of electron correlation and the approximation used to solve the Schrödinger equation. The energy calculations involve the following.

- Determination of the geometry of the molecule: To perform energy calculations, the 3D arrangement of the atoms that minimize the potential energy surface of the system needs to be known, and this can be done using NMR spectroscopy, X-ray crystallography, computational methods, etc.
- Basis set and functional selection: After the geometry has been optimized, the next step is to choose a suitable basis set and functional to calculate the system's energy. This

involves selecting an appropriate level of theory for the system.

- Defining electronic structure of the system: The distribution of specific electrons in the system is determined by methods such as the Hartree-Fock theory and the density functional theory. The electronic structure of the system is then calculated using the preselected method and basis set.
- Solvation model: If the system is in solution, a solvation model must be applied to consider the solvent's effect on the system's energy.
- Thermal effects: The energy of the system is then changed to account for things like zero-point energy and thermal motion, which are caused by heat.

After the energy calculation has been completed, post-processing may be undertaken to assess the results and extract relevant information, such as molecular orbitals, bond energies, reaction energies, and intrinsic parameters of the system.

2.9 Model and Method Used to Generate Trajectories

To simulate the pyrolysis of methyl stearate, computer models based on molecular dynamics (MD) were used. MD simulations are used to predict properties and reactions at the molecular level by simulating the behavior of atoms and molecules in a system. It is a technique that solves equations of motion for a system and returns trajectories that can be interpreted in various ways. MD simulations have been used to predict macroscopic behavior based on microscopic observations.[37,73–75]

Another approach that could have been used is the computer fluid dynamics (CFD); which is typically used to solve fluid flow-related problems, by using numerical methods and

computer algorithms to model fluid behavior on a larger scale and predict the macroscopic behavior such as temperature, mass transfer, flow patterns of fluids in a variety of applications.[76] Both types of simulations can provide useful information about methyl stearate pyrolysis, such as the rates and pathways of chemical reactions, distribution of heat and mass, and resulting products and byproducts.

The initial configuration of the system in a MD simulation of methyl stearate pyrolysis was created by placing the methyl stearate atoms in their positions and assigning velocities-based system temperature of 3500 K, with the standard time step for ADMP trajectories in Gaussian 16 set to 1 fs while using M06-2X density functional [5]. The simulation was performed by calculating the forces acting on each atom and using these data to update their positions and velocities over time. This would allow the simulation to monitor the progress of the pyrolysis reaction and provide information regarding the molecular properties of the system.[5] The M06-2X is a hybrid density functional that has been designed to perform well for large systems such as those containing hundreds of atoms. This can be useful for modeling complex chemical processes such as the pyrolysis of biomass or dissolution of proteins in solution.

Importance of the MO6-2X over other functionals:

i. Greater computational efficiency despite its improved accuracy, the M06-2X functional is generally more computationally efficient than the B3LYP functional. This can make it more practical for use in large-scale simulations or in cases requiring a rapid turnaround.
ii. Greater reliability for predicting absolute energies: The M06-2X functional provides more reliable predictions of absolute energies, which can be important for applications such as thermochemistry or reaction kinetics.[77]

iii. M06-2X is one of the best functionals for a broad range of applications on main group thermochemistry, kinetics, and noncovalent interactions.[78]

Overall, the M06-2X functional offers many potential benefits over the B3LYP functional, making it a useful tool for a wide range of chemical modeling applications.[52,77]

2.10 Statistical Analysis of Events

An in-house database of 200 ab initio trajectories was generated with a time step of 1 fs, an overall timeframe of 1000 fs, and a temperature of 3500 K. These trajectories were then observed for different fragments. A total of 111 trajectories dissociated and 99 did not. Of those that dissociated, up to 12 bond-breaking and/or bond-forming events were observed. In this study, only events 1–3 were analyzed due to being the most statistically significant events, going any further would have left us with very little data to analyze. Statistical analysis was performed to investigate the trends, patterns, and relationships between the logged events. A confidence limit of 95% was used.

A confidence interval is a range of intervals that explains the uncertainty in a range of values and provides the degree of confidence. A 95% confidence as shown in Figure 4 represents a level of certainty that there is only a 5% (i.e., the sum of the 2.5% outliers of the lower and upper limit) chance that the events observed were due to random noise. Confidence intervals were used to demonstrate the accuracy of the method. There are different confidence intervals used, for this study we used the 95% and 99% confidence intervals.

Figure 5 shows a sample with a confidence interval of 50%, each point in the row represents a sample with the same normal distribution. The colored lines represent 50%

confidence intervals for the mean, and the sample mean, denoted by a diamond, is at the center of each interval. For about 50% of the sample, you can see that most of the confidence interval passed through the population mean which blue, while for the other 50% which are the red ones, they did not pass through the population mean.

Alpha level's Z scores are usually used for two-tailed tests and are related to confidence interval value.[81] From Figure 6, the population mean value is 95% likely to be between z alpha/2 of ±1.96 standard deviations (z-scores) from the average which loosely translates to taking the mean ±1.96 standard deviations from the mean to find the upper and lower bound of the 95% confidence interval as a result, there is a 5% chance that the event average lies outside the upper and lower confidence intervals (as demonstrated by the 2.5% of outliers on either side of the 1.96 z-scores in Figure 4. To obtain an alpha value of 95%, you can use Table 2 to get the alpha, alpha/2 and specifically z alpha/2 value to give 1.96.

Then by using a Z-table in Table 3, we can then trace the row that has the ones digit and the tenth digit (1.9), then the column that has the hundredth digit of your z alpha/2 value (0.06), by intersecting both together, a z alpha/2 value of 1.96, then p value is 0.4570, which tells us the area under a curve up to or below the z score is 0.4570. This allows us to identify outliers and extreme values by looking for data that are standard deviations away from the mean. These outliers could be due to measurement error or other factors that are not a good representative of the complete dataset.

Table 2. Alpha, alpha/2, and Z alpha/2 for different confidence levels

Confidence Level	Alpha	Alpha/2	Z alpha/2
90%	10%	5.0%	1.645
95%	5%	2.5%	1.960
98%	2%	1.5%	2.326
99%	1%	0.5%	2.576

Table 3. Standard normal table Z, entries are the area under a curve between the mean and z standard deviation above the mean e.g., for z=1.96, the area under the curve between the mean and z is 0.4570

z	0.00	0.01	0.02	0.03	0.04	0.05	0.06	0.07
1.6	0.4452	0.4463	0.4474	0.4484	0.4495	0.4505	0.4515	0.4525
1.7	0.4554	0.4564	0.4573	0.4582	0.4591	0.4599	0.4608	0.4616
1.8	0.4641	0.4649	0.4656	0.4664	0.4671	0.4678	0.4686	0.4693
1.9	0.4713	0.4719	0.4726	0.4732	0.4738	0.4744	0.4750	0.4756
2.0	0.4772	0.4778	0.4783	0.4788	0.4793	0.4798	0.4803	0.4808

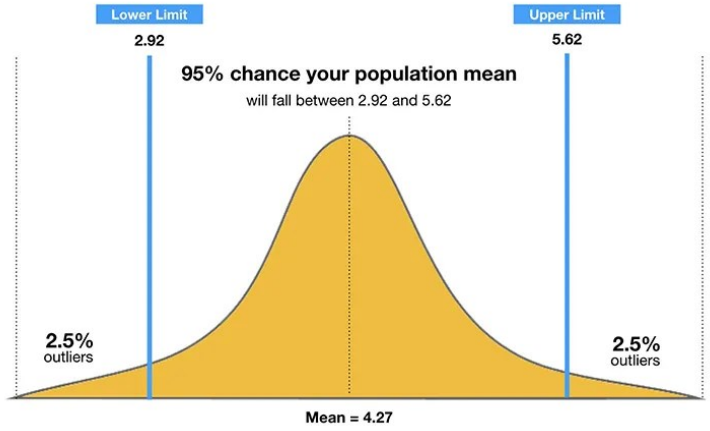

Figure 4. 95% Confidence interval i.e., 95% chance estimate will fall between the lower and upper limit[79]

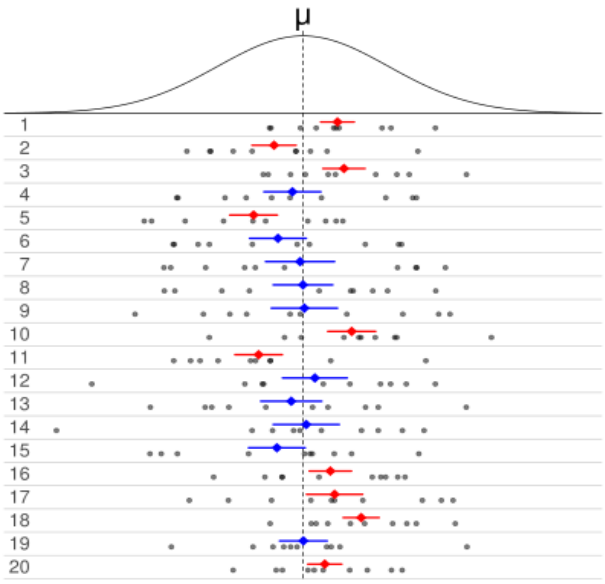

Figure 5. 50% confidence intervals for the mean of a normal distribution[80]

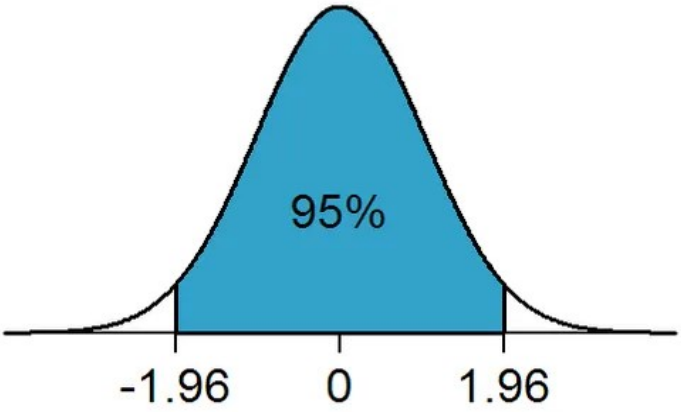

Figure 6. An alpha value of 1.96[79]

CHAPTER 3. RESULTS

3.1 Bond Scission of Methyl Stearate

Thermal cracking of methyl stearate is mostly dominated by homolytic bond cleavage, in which several products are formed, including gas-phase products, organic liquid products, and tar-like products. Two hundred trajectories of parent structure methyl stearate in Figure 7 were observed for dissociation; 101 (51%) trajectories dissociate, whereas 99 (49%) trajectories did not dissociate as shown in Figure 8.

Table 4 presents a record of fragments produced by dissociated methyl stearate trajectories, arranged in decreasing order of their frequency of occurrence. The table provides information on the fragments' names, their frequency of dissociation, and their molar masses in grams per mole. These fragments are identified as the products resulting from the simulation process. Figure 9 displays the fragments that emerged as molecular weight increased, with hydrogen representing the smallest fragment and $C_{19}H_{37}O_2$ radical being the largest fragment. These products were characterized by: Inorganic gases including, CO and CO_2; carbonyls; radicals; C1-C19 alkanes and alkanoates, with Hydrogen radical formed with the highest frequency, these products were found to be similar to those observed in experimental pyrolysis of methyl stearate.[82] Figure 9 shows the frequency of fragments forms as molecular weight increases. The trajectories that dissociated in Figure 8, were labeled, then monitored, and specific events that led to their dissociation were logged.

3.2 Bond-breaking and Bond-forming Event

Each carbon and oxygen atom were assigned an atom number, as shown in Figure 7 to

accurately describe the events occurring in each reactive simulation. These logged events were characterized by bond-breaking and bond-forming events of atoms for each of the jobs. The largest number of events observed in a single trajectory was 13 as shown in Figure 10 consisted of:

1. Bond breaking between C1 and the β- O20 at time 21 fs.
2. Bond breaking between C1 and C1-H at time 21 fs.
3. Bond forming between C1-H and 0-21 at time 25 fs.
4. Bond breaking between C18 and C19 at time 138 fs.
5. Bond forming between C18 and C19 at time 166 fs.
6. Bond breaking between C15 and C16 at time 384 fs.
7. Bond forming between C15 and C16 at time 418 fs.
8. Bond breaking between C13 and C14 at time 376 fs.
9. Bond forming between C13 and C14 at 412 fs.
10. Bond breaking between C16 and C17 at 432 fs.
11. Bond forming between C16 and C17 at 489 fs.
12. Bond breaking between C15 and C16 at 501 fs.
13. Bond forming between C15 and C16 at 545 fs.

3.3 Interpreting Statistical Analysis of Logged Events

For an observed event i, its probability Pr (i) can be expressed as:

$$Pr(i) = \frac{N_{obs}(i)}{N_{total}} \tag{13}$$

where $N_{obs}(i)$ is the number of times an event (i) was observed

N_{total} is the total number of observed events.

while the variance at confidence limit (C.L.) of 95% (Z = 1.96) can be expressed as:

$$Variance(\sigma) = (Z)\sqrt{\frac{Pr(i) \times Pr\,(\neq i)}{N_{total}}} \tag{14}$$

where $Pr(i)$ is determined from Equation 13, and $Pr\,(\neq i)$ is the probability of an event that is not equal to i.

For the first set of events in all the jobs observed, which were breaking events between C, H, and O, each atom position was logged with its time of occurrence. A statistical analysis was conducted to calculate the standard deviation of the time of occurrence for a set of similar events. The mean time of occurrence was used as the central tendency measure to compute the standard deviation. The dispersion of the time of event occurrence was determined by comparing the magnitude of the standard deviation to the mean. Events with a variance that exceeded their probability, as indicated by a variance greater than "Pr (i)" were excluded from the analysis. This decision was based on the assumption that such events were outliers, meaning they were not representative of the total set of events under consideration. By excluding these outliers, the statistical analysis was being conducted on a more representative and reliable dataset. Pr (i) and variance were first calculated with an N_{total} of 101 trajectories that dissociated as shown in the 4th and 5th column with the 6th and 7th column representing Pr (i) and variance based on an N_{total} of 200 trajectories which were the total trajectories that we started with, and subsequent events were analyzed based off these total 200 trajectories. A C.L. of 95% (Z= 1.96) was used and only six events were found to be significant, i.e., 95% chance they did not occur by random chance,

which were those that only had their Pr (i) values greater than the variance, only significant events were further analyzed for significant events, which we call event 2 herein. Based on the significance of initiation step in a series of subsequent chemical reactions (Event 2), only six events were determined to be statistically significant. These significant events were identified in Table 5. Event 1 involved only breaking events, while Event 2 and 3 consisted of breaking and forming events as shown in Table 6.

In Figure 11, the solid lines from the parent structures represent event 1, with the cable dash lines leading to event 2, finally the dashed double lines leading to event 3. For the first significant event observed, there was a bond breaking between C1 and O20, then a bond breaking between C2 and C3, which then led to a bond forming between C1 and 020. Another look at the third event shows C1-O20 breaking, then subsequent reforming, which then led to C2-C3 and C3-C4 breaking in the third event series. It is observed that the further we go down the event series, the less significant events are observed, and for the purpose of this study, we curtailed our analysis to focusing on three events, which allows us to develop more robust statistical models. Focusing on a smaller subset of data during analysis enables the development of more dependable models capable of predicting system behavior under diverse conditions.

3.4 Bond Dissociation Energy Determination

The trajectories containing the individual fragments that dissociated and formed were given new identifiers namely molecules "named" as numbers 1-15 as shown in Figure 12, molecule 1 being the parent reactant that results in the subsequent products and are saved as "xyz" files. In the first chemical equation, molecule 1 (the parent structure of "methyl stearate") broke into reaction 1 to give 2 (an acetate radical) and 3 (heptadecane radical). In reaction 3, 1

also breaks into 8 (methyl radical) and 9 (octadecenoate radical), then 9 proceeded to break into 10 (carbon dioxide) and 3 (heptadecane radical), then molecules 10 and 8 combine to form 2, which is an acetate radical. These "xyz" files contained specific information on the exact atoms that broke, what kinds of products were formed, and the resulting structure. The "xyz" files were then converted into "gif files" and fed into the Gaussian 16 suite of programs to run thermochemistry calculations, using the M06-2X/6-31+G (d, p) level of theory with individual files running for about 8 hours depending on the content of the file; namely molecules 1 through 15, with 1 being the parent reactant that results in the overall fragmentation.

Once the calculations are performed, then Gaussian outputs a "notebook" document containing information such as the chemical structure's entropy, free energy, electronic energy, and zero-point energy correction calculations. These output files were then analyzed to determine thermochemical information for each step of the reaction. Reaction 1, 2,5,6 and 7 which involve a single step reaction in which a bond is being broken can be described using BDE values while reactions 3 and 4 which involve multistep reactions and involve multiple bonds being broken. The products of these reactions cannot be characterized by BDE values as they involve the interaction of multiple bonds and the formation of new products. Multistep reactions are typically described using reaction mechanisms. BDE values can be used to predict the reaction rates and their thermodynamic pathways.[83]

To determine a Bond Dissociation Energy value, consider the following example reaction:

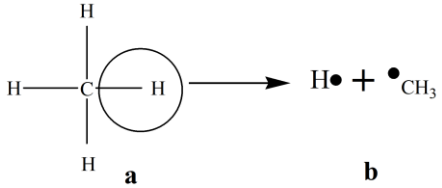

B.D.E of the above reaction = 627.51(E_b-E_a) kj/mol

Where E_a is the Electronic Energy $(EE)_a$ + Zero Point Energy Correction $(ZPEC)_a$,

E_b is the Electronic Energy $(EE)_b$ + Zero Point Energy Correction $(ZPEC)_b$

3.5 Reaction Pathway with Calculated BDEs for Single Step Reactions Involving Carbon

As shown in Figure 13, molecule 1 dissociated into several other molecules which represent specific fragments that were formed during the simulation. A compilation of reactions was made, and the bond dissociation energies (BDEs) for the corresponding single step reactions were determined. The highest BDE value of 201.7 kcal/mol was observed for the formation of molecule 12 in reaction 4, as depicted in Figure 13. The high BDE value indicates that the formation of the methylene radical is highly endothermic, requiring a substantial amount of energy to break the bond. This suggests that 12 is likely an intermediate species in a multistep reaction pathway, rather than a stable product. The predominant mechanism in the thermal cracking of methyl stearate involves radical formation through C-H abstraction and C-C bond breaking, with some C-O bonds breaking as well.[26] The BDE values for the C-C bond dissociation were then compared to the previously determined BDEs, as shown in Table 7.

3.6 Testing Accuracy of Study by Comparison to Other Works

In the simulation of saturated methyl stearate, the C-C bond dissociations were analyzed. The easiest bond to break was C3-C4, with a BDE of 82.6 kcal/mol, followed by C6-C7 with a BDE of 84.8 kcal/mol, then C5-C6 with a BDE of 86.4 kcal/mol, C4-C5 with BDE of 87.8 kcal/mol, and C1-O20 with a high BDE of 91.0 kcal/mol. The hardest bond to break was between the carbonyl carbon C2 and C3, with a BDE of 94.7 kcal/mol. To ensure the accuracy

and reliability of our results, we conducted a comparative analysis of our BDE calculations with those from other studies. The maximum absolute difference observed was approximately 2.3 kcal/mol, as detailed in Table 7.[5,26] Figure 3 shows the numbering of the specific carbon atoms that has been compared. Our comparison was carried out using a different methodology than theirs, specifically, the B3LYP/6-31G (d, p) density functional and empirical atomic increments were used to determine the gas-phase standard enthalpy of formation at 298.15 K in these studies. In contrast, we employed the M06-2X/6-31+G (d, p) method to determine the bond dissociation energies (BDE) for C-C bonds. This comparison allowed us to verify the accuracy of our approach and to ensure that our results were consistent with those obtained using other methodologies.[26]

3.7 Human/Computer Identification of Events in Methyl Stearate Reactivity

This study analyzed 200 trajectories of methyl stearate, which approaches the limit of human readable sample sizes. Thus, there is a need to programmatically log events. Others in the Siebert group have produced a development version of such a computer program. The manually logged events were then compared to the computer-determined events which were analyzed using the Jupyter Notebook (an open-source web-based application used to create and share computational documents). The computer code showed high efficiency in flagging events with those discrepancies corresponding to “near to end” events that typically take place around 994-1001 fs as shown in Figure 15. The code also succeeded in flagging events that were missed when viewing and logging events with the human eye like H-abstraction and C-H bond forming.

Several heuristics were optimized to make the automatically generated events very close to the manually generated ones. Table 8 shows that of the 200 trajectories that were analyzed, the

computer and the human eye agreed that 46 of those trajectories had events happening, while also agreeing that 92 of the trajectories did not have any form of event happening, with 7 false positives and 2 false negatives. The remaining 53 trajectories had bond-breaking right at the end of the simulation, and the computer did not flag those events.

To better understand why the computer could not flag these "near to end" events, we wrote another code that printed out the bond distances, and bond velocity over time for each individual bond in a trajectory as shown in Figure 15, the bonds were shown to vibrate around their position then finally broke at the end, without enough mechanistic information to determine there was a bond dissociation over the course of 1001 fs of the simulation, due to a smaller time frame and computational cost.

3.8 Trajectory Bond Distance Over Time

Furthermore, for the 46 trajectories that had agreement between computer-generated events and the human eye, we looked at specific events that were similar in both instances. It was observed in Figure 16 that for the bond dissociation events, the average bond distance for C-C, C-O, C-H and H-O atoms for methyl stearate was higher in human as compared to the computer, this is the point where the interaction between the atoms does not exist. It was predicted that the bond forming for the computer-generated events would have a higher bond distance than humans, as shown in Figure 17, where the average bond distance for the computer was higher than that for humans except, in H-H and C-O forming events, in which only one and three individual events were analyzed to obtain the average.

Table 4. Fragments were generated from methyl stearate trajectories that dissociated, with decreasing frequency of occurrence based on their respective molar masses

Fragments	Frequency of dissociation	Molar mass (g/mol)	Fragments	Frequency of dissociation	Molar mass (g/mol)
H	29	1.008	$C_{12}H_{24}$	2	168.319
CH3	20	15.03	$C_{13}H_{25}O_2$	2	213.33
$C_{17}H_{35}$	14	239.45	$C_{13}H_{26}$	2	182.34
CH	13	13.02	$C_{15}H_{28}O_2$	2	240.38
CO_2	12	44.01	$C_{16}H_{32}$	2	224.42
$C_{19}H_{37}O_2$	10	297.49	$C_{16}H_{34}$	2	226.41
$C_4H_7O_2$	10	87.1	$C_{17}H_{33}O_2$	2	269.43
C_4H_9	9	57.11	CH_4O	2	32.04
$C_{13}H_{27}$	8	183.35	C_2H_2	2	26.04
$C_{15}H_{31}$	6	211.4	C_2H_2O	2	42.04
$C_{17}H_{34}$	6	238.5	C_2H_4O	2	44.05
$C_{18}H_{35}O_2$	6	283.46	$C_2H_4O_2$	2	60.05
CH_2O	6	30.03	C_2H_5	2	29.06
C_5H_{11}	6	71.14	C_2HO	2	30.03
$C_{15}H_{29}O_2$	5	241.38	$C_3H_5O_2$	2	73.07
$C_{12}H_{25}$	5	169.32	$C_3H_6O_2$	2	74.08
C_8H_{17}	5	113.22	$C_4H_8O_2$	2	88.11

Table 4 Contd. Fragments were generated from methyl stearate trajectories that dissociated, with de-creasing frequency of occurrence based on their respective molar masses

Fragments	Frequency of dissociation	Molar mass (g/mol)	Fragments	Frequency of dissociation	Molar mass (g/mol)
$C_{11}H_{21}O_2$	4	185.28	$C_5H_9O_2$	2	101.12
$C_{14}H_{27}O_2$	4	227.36	C_6H_{12}	2	84.16
$C_{14}H_{29}$	4	197.37	$C_6H_{12}O_2$	2	116.16
$C_{15}H_{30}$	4	210.4	$C_9H_{17}O_2$	2	157.23
$C_2H_3O_2$	4	59.04	CH_2	2	14.03
C_2H_4	4	28.05	CH_3O	2	31.03
C_3H_6	4	42.08	CHO	2	29.02
$C_5H_8O_2$	4	100.11	$C_{11}H_{20}O_2$	1	184.27
H_2	4	2.016	$C_{19}H_{38}$	1	226.49
$C_{10}H_{19}O_2$	3	171.25	C_5H_9	1	69.12
$C_{16}H_{33}$	3	225.42	C_7H_{12}	1	96.17
C_9H_{19}	3	127.24	C_7H_{13}	1	97.18
$C_{10}H_{21}$	2	141.27	C_7H_{14}	1	98.19
$C_{11}H_{22}$	2	154.29	$C_7H_{14}O_2$	1	130.18
$C_{11}H_{24}$	2	156.31	C_7H_{15}	1	99.19
$C_{12}H_{23}O_2$	2	199.3			

Table 5. Analysis of significant occurrences in initiation step with 95% confidence interval based off 200 sum trajectories analyzed (dissociated + undissociated)

Atom position	Atom type	N_{obs}	Pr(i)	Var.	Pr(i)	Var.	Avg(T)	Stdev (T)
			$N_{total} = 101$		$N_{total} = 200$			
1,20	C-O	27	26.70%	6.10%	13.50%	4.70%	192.9	238.4
2,3	C-C	12	11.90%	4.50%	6.00%	3.30%	209.1	272.2
15,16	C-C	12	11.90%	4.50%	6.00%	3.30%	615.8	462.1
4,5	C-C	10	9.90%	4.10%	5.00%	3.00%	746.5	264.7
6,7	C-C	7	6.90%	3.50%	3.50%	2.50%	625.6	341.9
3,4	C-C	7	6.90%	3.50%	3.50%	2.50%	344.1	311.3
5,6	C-C	5	5.00%	3.00%	2.50%	2.20%	733.0	419.4
14,15	C-C	3	3.00%	2.40%	1.50%	1.70%	998.3	4.619
1-1H	C-H	3	3.00%	2.40%	1.50%	1.70%	135.3	99.90
10,11	C-C	3	3.00%	2.40%	1.50%	1.70%	995.7	9.238
11,12	C-C	3	3.00%	2.40%	1.50%	1.70%	936.7	108.8
7,8	C-C	2	2.00%	1.90%	1.00%	1.40%	991.5	13.43
13,14	C-C	2	2.00%	1.90%	1.00%	1.40%	997.0	0

Table 6. Significant event from initiation events, leading to events 2 and 3, with probability greater than variance

Atom position	Atom type	Break or form	N_{obs}	Pr($\boldsymbol{i}$)	Var.
		Event 2			
2,3	C-C	break	11	44.00%	19.50%
1,20	C-O	form	12	48.00%	19.60%
2,3	C-C	form	7	70.00%	28.40%
3,4	C-C	form	2	50.00%	49.00%
6,7	C-C	form	3	50.00%	40.01%
15,16	C-C	form	5	83.33%	29.82%

Table 6 Contd. Significant event from initiation events, leading to events 2 and 3, with probability greater than variance

Event 3					
Atom position	Atom type	Break or form	$\mathbf{N_{obs}}$	$\mathbf{Pr(i)}$	**Var.**
3,4	C-C	break	4	33.33%	26.67%
2,3	C-C	break	5	41.67%	27.89%
6,7	C-C	break	2	66.67%	53.34%

Table 7. Comparison of standard enthalpy of reaction of C-C bond breaking[5,26]

		This work BDE (kcal/mol)	Other works BDE (kcal/mol)		
Molecule no.	Atom position	Methyl stearate	Methyl palmitate	Methyl Palmitoleate	Methyl Oleate
12 & 13	C15-C16	85.1	86.8	86.6	87.8
14&15	C6-C7	84.8	87.1	86.9	87.9
4 & 5	C4-C5	87.8	86.8	86.5	87.7
4 & 5	C5-C6	86.4	86.5	86.52	87.9
10 & 11	C3-C4	82.6	82.9	82.6	85.0

Table 8. Comparison of computer and human generated events with a dist_after_multiple of 1.00 to determine the extent of agreement

1.00			
		Human Eyes	
		Event	Non-Event
Computer Generated	Event	46	7
	Non _event	2	92
No. of false positives = 7			
No. of false negatives = 2			

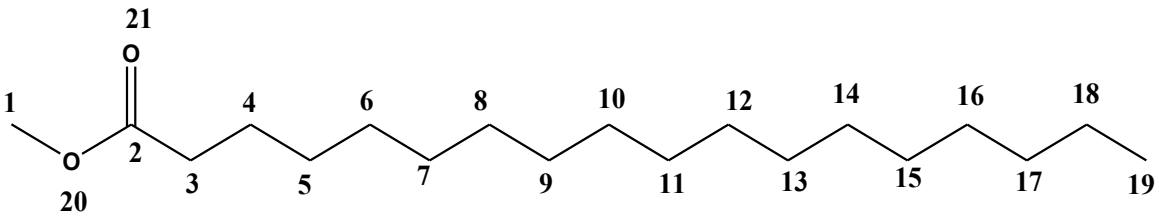

Figure 7. Structure and labeling of atomic positions in the methyl stearate structure; numbers will be used to describe where bond-breaking and bond-forming occurred

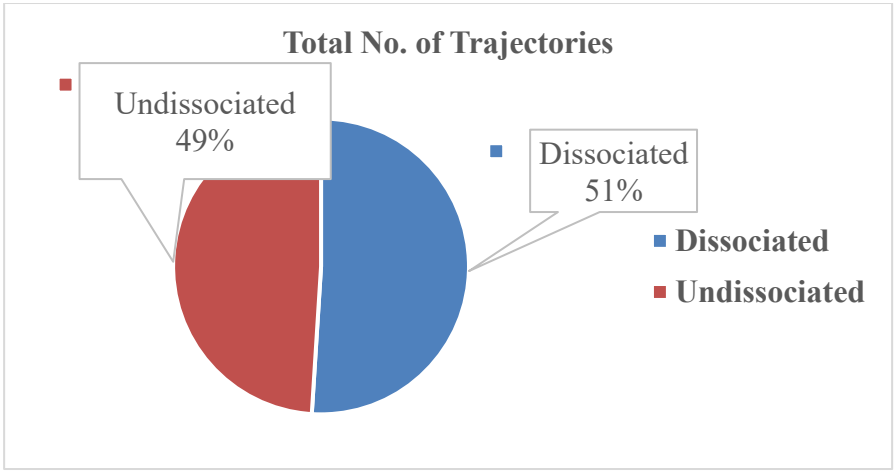

Figure 8. Total number of trajectories that dissociated; trajectories that dissociated were then analyzed for significant events

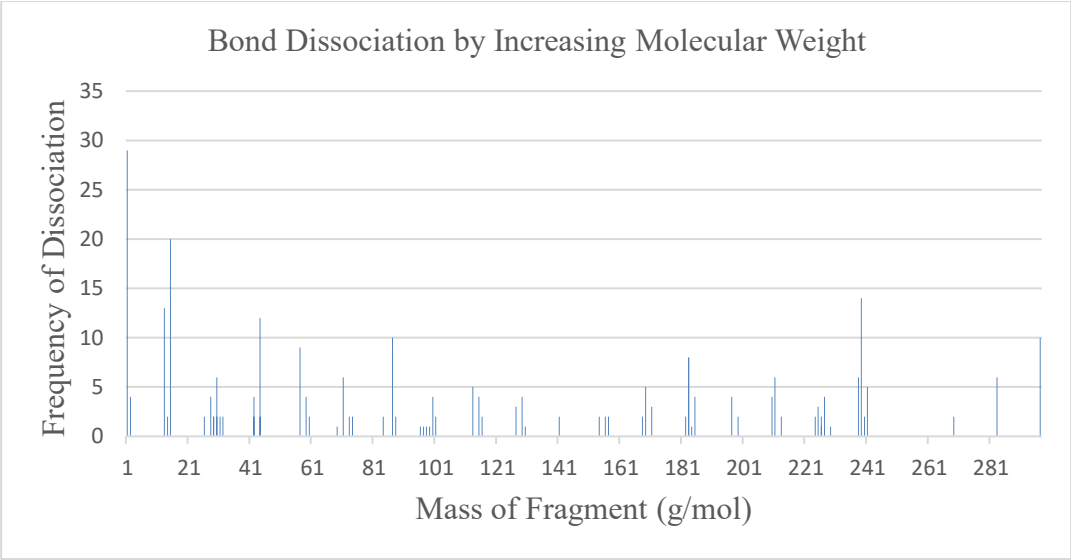

Figure 9. Fragments formed from the simulation of pyrolysis process with increasing molecular weight of the products

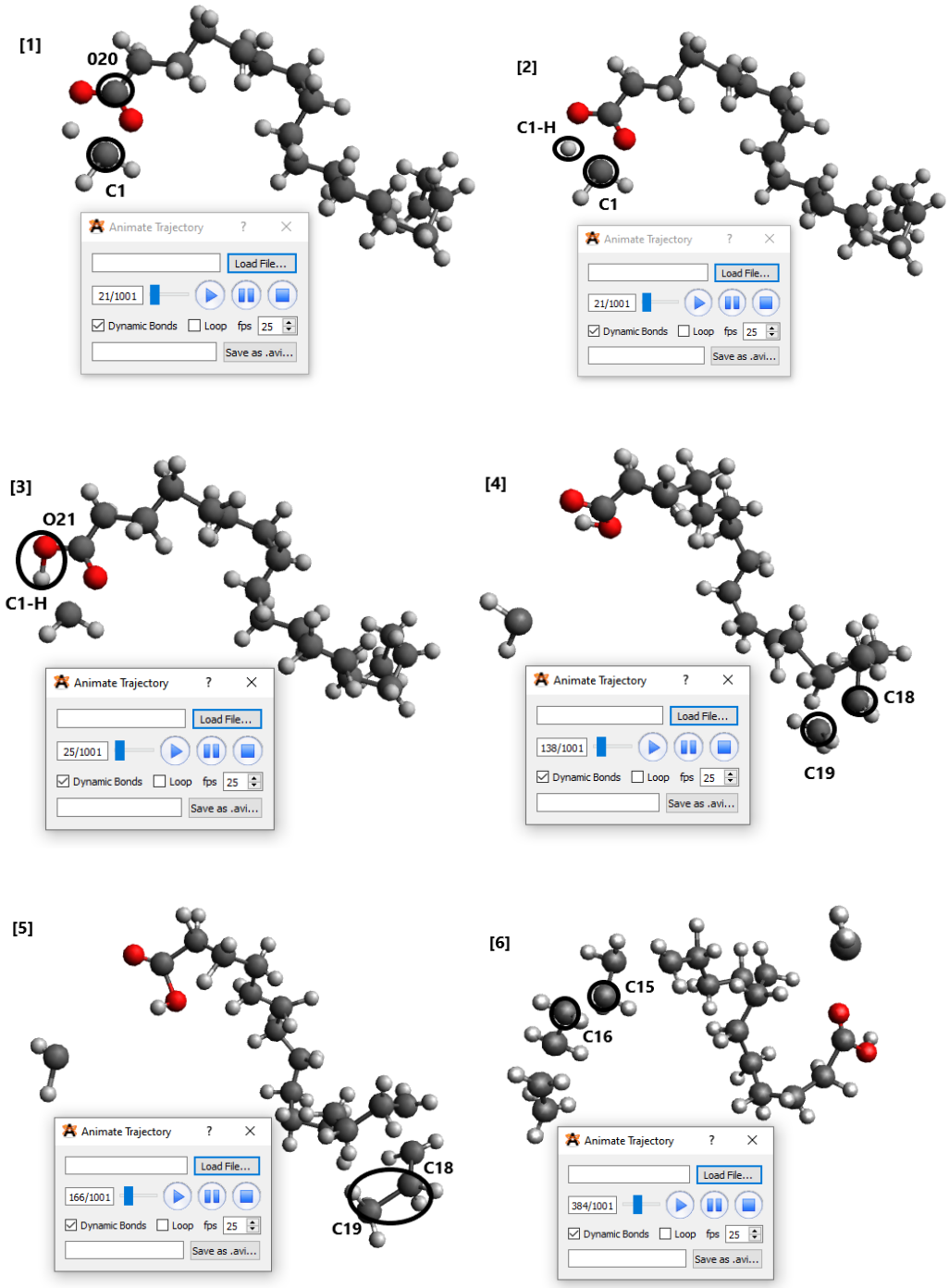

Figure 10. Snapshots of the single most reactive trajectory (13 total events)

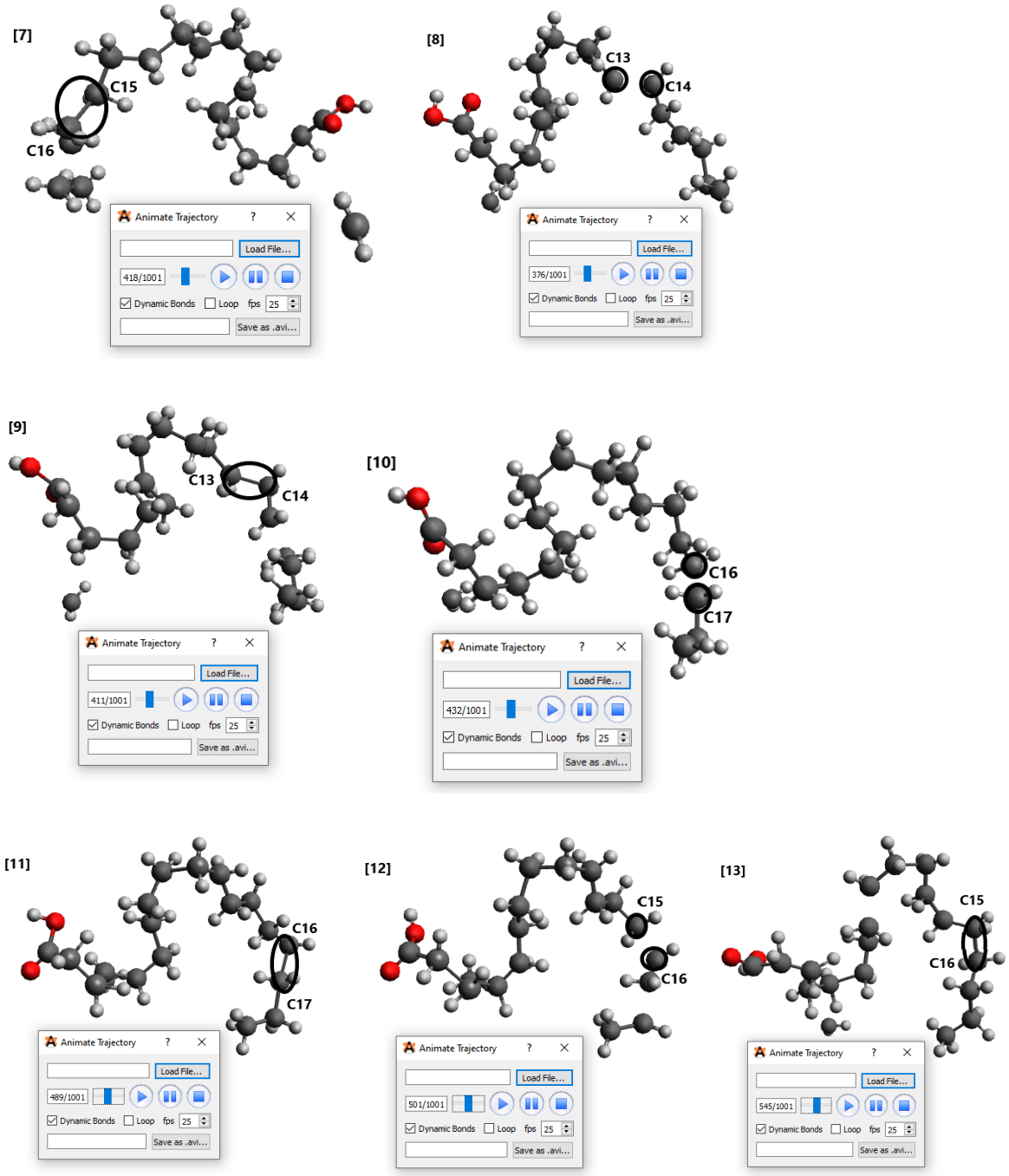

Figure 10 Contd. Snapshots of the single most reactive trajectory (13 total events)

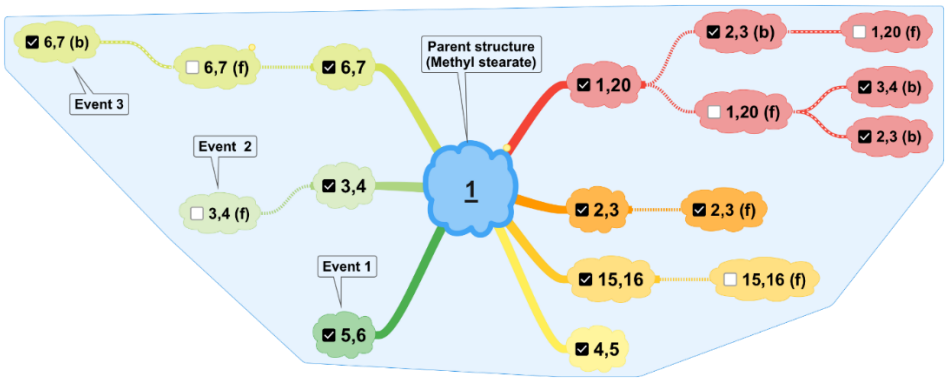

Figure 11. Progression of significant breaking/forming event from the parent structure, through event 1 to 3

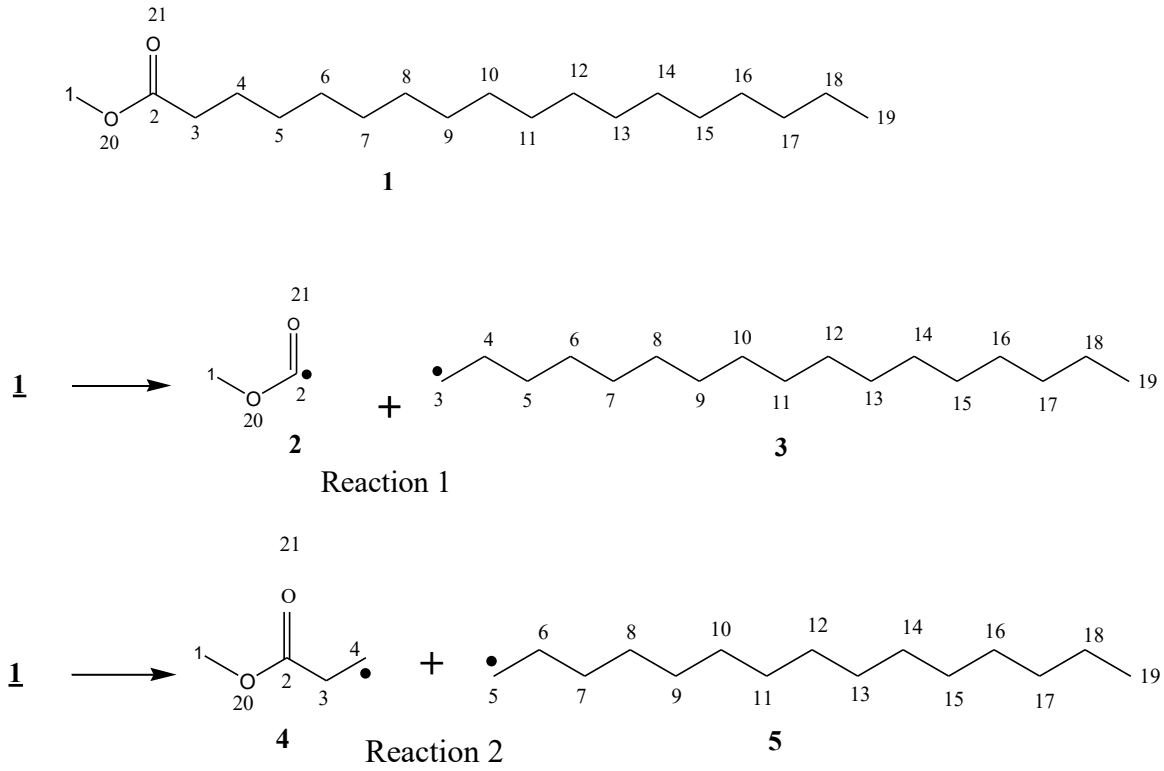

Figure 12. Significant bond dissociation pathways in methyl stearate

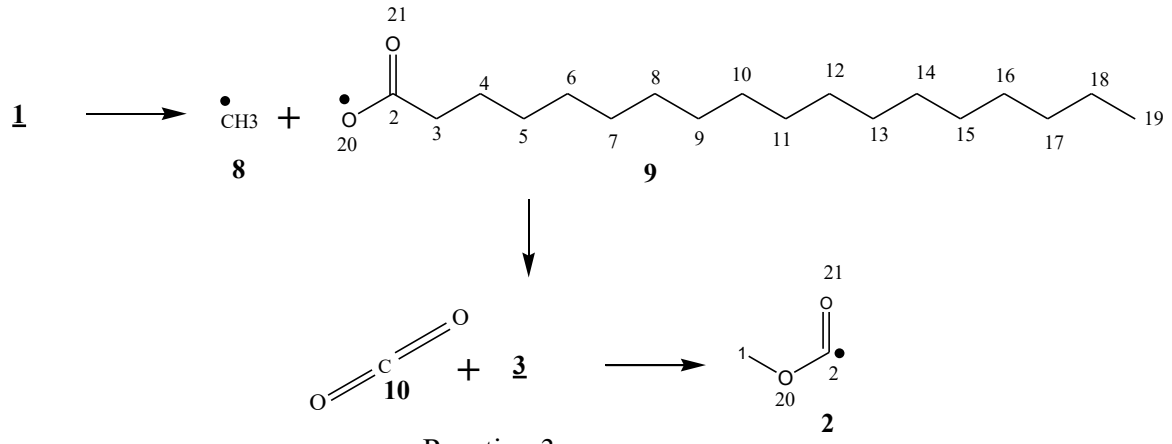

Reaction 3

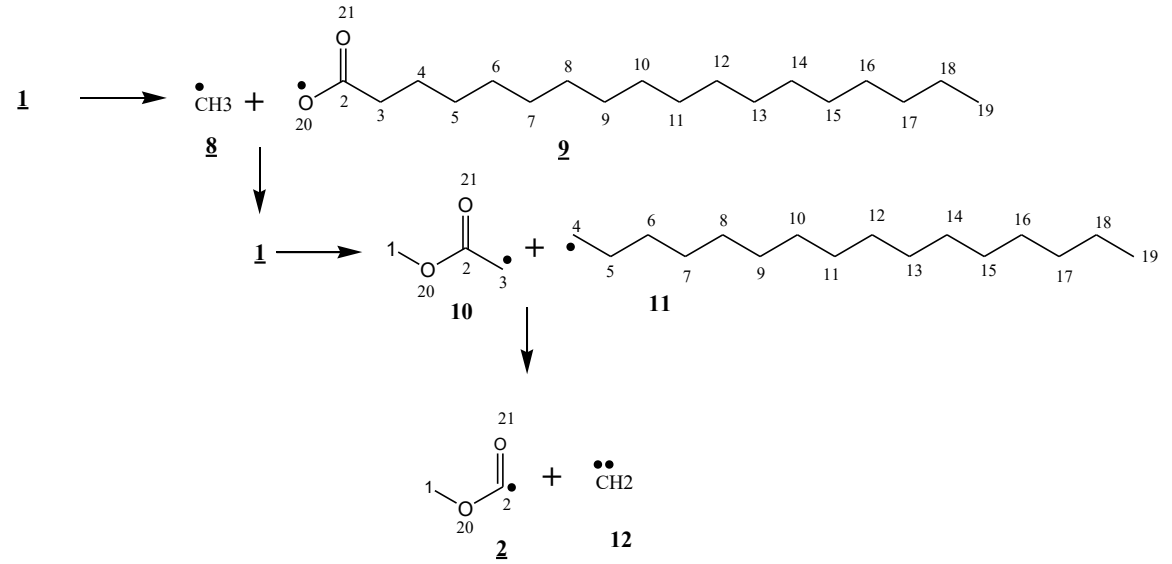

Reaction 4

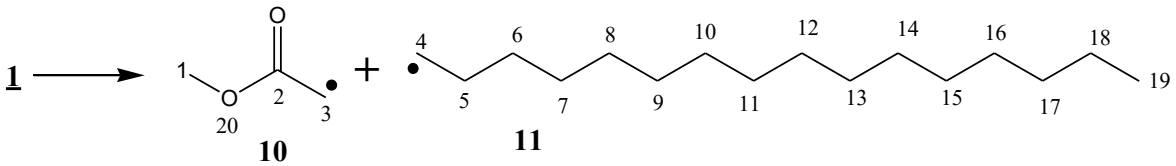

Reaction 5

Figure 12. Contd. Significant bond dissociation pathways in methyl stearate

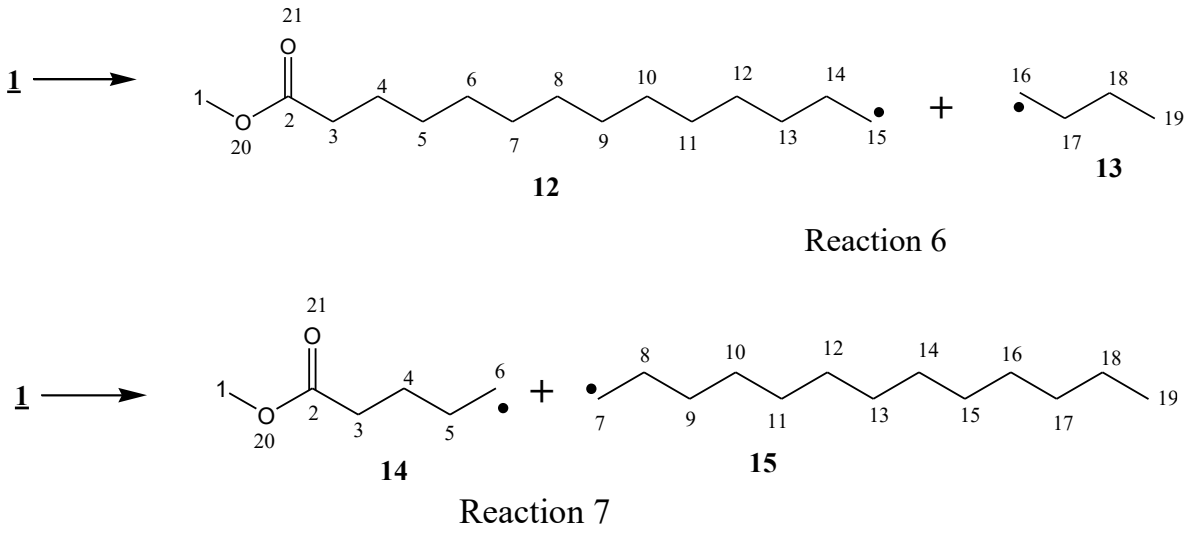

Figure 12. Contd. Significant bond dissociation pathways in methyl stearate

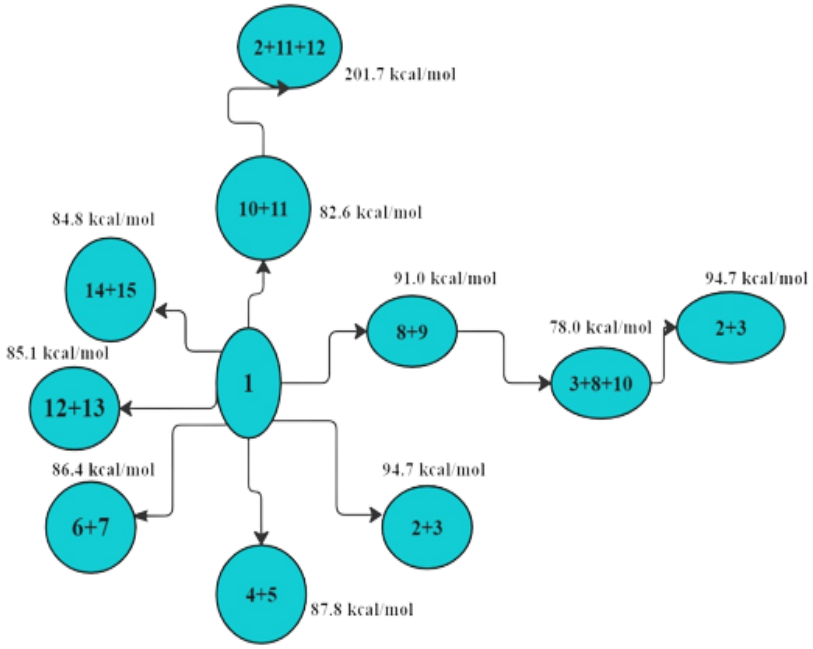

Figure 13. Reaction pathway and B.D.E of reactions showing respective reaction numbers

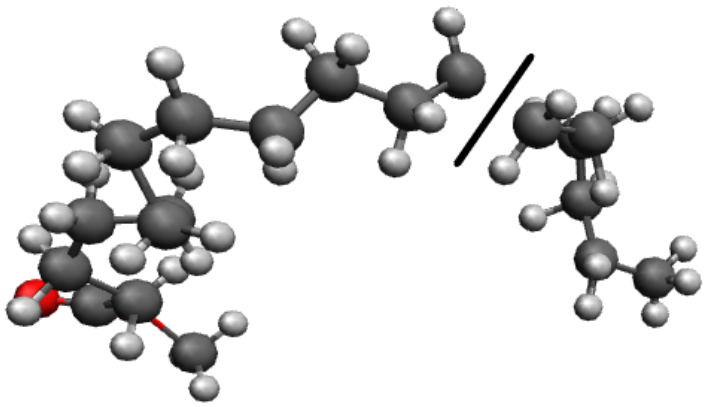

Figure 14. An illustration of bond breaking between two carbon atoms

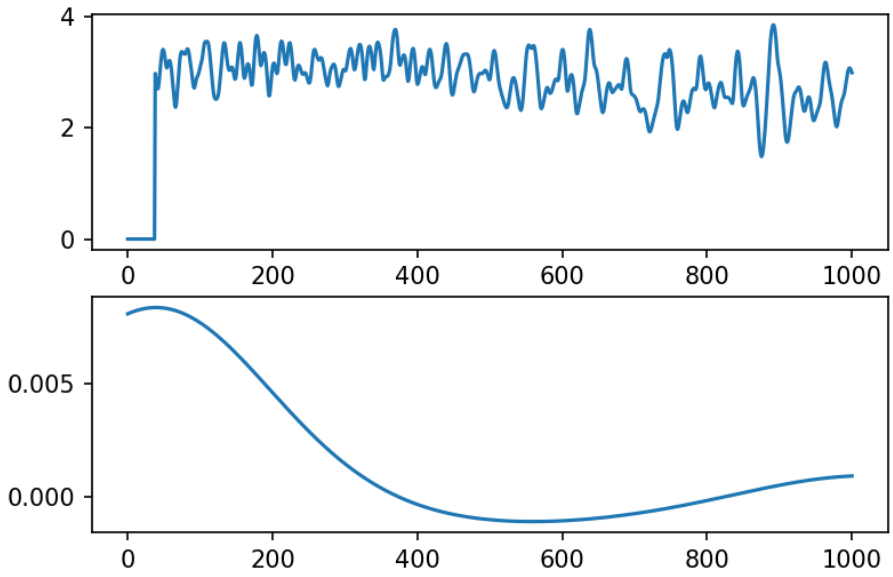

Figure 15. A plot of bond distance over time and velocity/time observed for bond breaking in a single trajectory

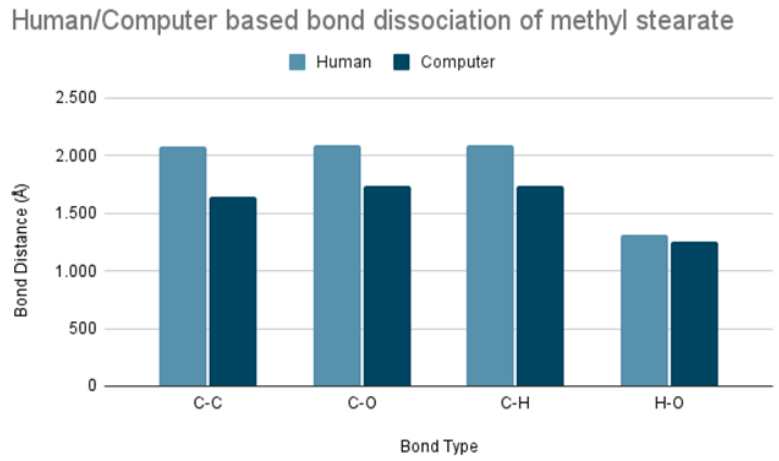

Figure 16. Computer/Human based monitoring bond dissociation in methyl stearate

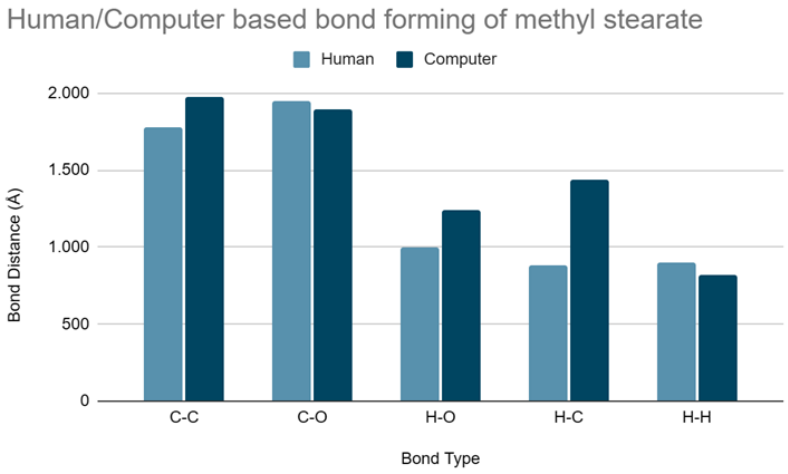

Figure 17. Computer/Human based monitoring of bond forming in methyl stearate

CHAPTER 4. CONCLUSION

This work involves a comparison between theoretical investigations and other studies of methyl stearate pyrolysis over 1.0 ps and at a temperature of 3500 K using the density functional M06-2X and a basis set at 6-31+G (d, p). Existing data on the thermal decomposition of methyl stearate showed significant agreement with molecular simulations of the pyrolysis of methyl stearate, indicating the potential for this method to be applied to other FAMEs. The analysis of bond dissociation energy and products revealed that the most common product of methyl stearate pyrolysis was hydrogen radicals due to H abstraction. Additionally, the β carbon had the lowest BDE and was more susceptible to breaking due to its proximity to the carbonyl. The BDEs calculated for products observed in this study were compared to other experimental works and showed excellent agreement.[5,26]

While the simulation and code used to generate events for methyl stearate showed some limitations, with further development and calibration, it has the potential to optimize reaction conditions for the dissociation of FAMEs into useful industrial components. The simulation's code that was written could not detect near-to-end events in thermal cracking of methyl stearate, causing false positives and negatives in

Table . Adjusting the break threshold and revising the conditional statement with a time frame can improve detection of these events. Furthermore, the code will need to be tweaked and require extensive validation and calibration against experimental data, also tested for other FAMEs and for larger molecules like triglycerides.

Overall, molecular structure can have a substantial effect on its dissociation pathways during pyrolysis and other chemical reactions if we can predict and comprehend the specific molecular features that influence dissociation and control reaction products and optimize reaction conditions for the dissociation of FAMEs into useful industrial components that can be used to efficiently serve as an alternative energy source.[37]

REFERENCES

(1) Khan, S.; Tripathi, A. K.; Srivastava, R.; Saleem, M. S.; Yeremenko, S.; Sydorenko, V. Bioremediation of Petroleum Contamination: A Short Review. *Ecological Questions*. 2022. https://doi.org/10.12775/EQ.2022.012

(2) U.S. Energy Information Administration. Electric Power Monthly. *Department of Energy*. https://www.eia.gov/electricity/monthly/ (accessed 2023-04-23).

(3) Zamba, Z. Z.; Reshad, A. S. Synthesis of Fatty Acid Methyl Ester from Croton Macrostachyus (Bisana) Kernel Oil: Parameter Optimization, Engine Performance, and Emission Characteristics for Croton Macrostachyus Kernel Oil Fatty Acid Methyl Ester Blend with Mineral Diesel Fuel. *ACS Omega* 2022, *7* (24), 20619–20633. https://doi.org/10.1021/acsomega.2c00682.

(4) Dresselhaus, M. S.; Thomas, I. L. Alternative Energy Technologies. *Nature* 2001, *414*, 332–337.

(5) Wilson, Z. R.; Siebert, M. R. Methyl Linoleate and Methyl Oleate Bond Dissociation Energies: Electronic Structure Fishing for Wise Crack Products. *Energy and Fuels* 2018, *32* (2), 1779–1787. https://doi.org/10.1021/acs.energyfuels.7b02798.

(6) Zhang, Z.; Yan, K.; Zhang, J. ReaxFF Molecular Dynamics Simulations of the Initial Pyrolysis Mechanism of Unsaturated Triglyceride. *J. Mol. Model* 2014, *20* (3). https://doi.org/10.1007/s00894-014-2127-6.

(7) Hu, Q.; Sommerfeld, M.; Jarvis, E.; Ghirardi, M.; Posewitz, M.; Seibert, M.; Darzins, A. Microalgal Triacylglycerols as Feedstocks for Biofuel Production: Perspectives and Advances. *Plant Journal*. 2008, *54*, 621–639. https://doi.org/10.1111/j.1365-313X.2008.03492.x.

(8) Standard Specification for Biodiesel Fuel Blend Stock (B100) for Middle Distillate Fuels. *Standard D02.E0, ASTM International*. West Conshohocken 2015.

(9) Zhang, Y.; Wang, X.; Li, Q.; Yang, R.; Li, C. A ReaxFF Molecular Dynamics Study of the Pyrolysis Mechanism of Oleic-Type Triglycerides. *Energy and Fuels* 2015, *29* (8), 5056–5068. https://doi.org/10.1021/acs.energyfuels.5b00720.

(10) Osmont, A.; Yahyaoui, M.; Catoire, L.; Gökalp, I.; Swihart, M. T. Thermochemistry of C-O, (CO)-O, and (CO)-C Bond Breaking in Fatty Acid Methyl Esters. *Combust Flame* 2008, *155* (1–2), 334–342. https://doi.org/10.1016/j.combustflame.2008.06.007.

(11) Osmont, A.; Catoire, L.; Dagaut, P. Thermodynamic Data for the Modeling of the Thermal Decomposition of Biodiesel. 1. Saturated and Monounsaturated FAMEs. *J. Phys. Chem.* 2010, *114* (11), 3788–3795. https://doi.org/10.1021/jp904896r.

(12) Luo, Y.; Ahmed, I.; Kubátová, A.; Šťávová, J.; Aulich, T.; Sadrameli, S. M.; Seames, W. S. The Thermal Cracking of Soybean/Canola Oils and Their Methyl Esters. *Fuel Process Technol.* 2010, *91* (6), 613–617. https://doi.org/10.1016/j.fuproc.2010.01.007.

(13) Sawangkeaw, R.; Bunyakiat, K.; Ngamprasertsith, S. A Review of Laboratory-Scale Research on Lipid Conversion to Biodiesel with Supercritical Methanol (2001-2009). *J. Supercrit. Fluids* 2010, *55* (1), 1–13. https://doi.org/10.1016/j.supflu.2010.06.008.

(14) Oyeyemi, V. B.; Keith, J. A.; Carter, E. A. Accurate Bond Energies of Biodiesel Methyl Esters from Multireference Averaged Coupled-Pair Functional Calculations. *J. Phys. Chm.* 2014, *118* (35), 7392–7403. https://doi.org/10.1021/jp412727w.

(15) Moser, B. R. Influence of Blending Canola, Palm, Soybean, and Sunflower Oil Methyl Esters on Fuel Properties of Biodiesel. *Energy and Fuels* 2008, *22* (6), 4301–4306. https://doi.org/10.1021/ef800588x.

(16) Li, X.; Xu, X.; You, X.; Truhlar, D. G. Benchmark Calculations for Bond Dissociation Enthalpies of Unsaturated Methyl Esters and the Bond Dissociation Enthalpies of Methyl Linolenate. *J. Phys. Chm.* 2016, *120* (23), 4025–4036. https://doi.org/10.1021/acs.jpca.6b02600.

(17) Knothe, G.; Steidley, K. R. A Comparison of Used Cooking Oils: A Very Heterogeneous Feedstock for Biodiesel. *Bioresour. Technol.* 2009, *100* (23), 5796–5801. https://doi.org/10.1016/j.biortech.2008.11.064.

(18) Knothe, G. "Designer" Biodiesel: Optimizing Fatty Ester Composition to Improve Fuel Properties. *Energy and Fuels* 2008, *22* (2), 1358–1364. https://doi.org/10.1021/ef700639e.

(19) Sheehan, J.; Camobreco, V.; Duffield, J.; Graboski, M.; Shapouri, H. An Overview of Biodiesel and Petroleum Diesel Life Cycles; 1998. http://www.doe.gov/bridge.

(20) Dhiraj Darunde; Mangesh D. Biodiesel Production From Animal Fats And Its Impact On The Diesel Engine With Ethanol-Diesel Blends: A Review. *Int. J. Emerg. Technol. Adv. Engin.* 2012, *2* (179).

(21) Pogaku, R.; Raman, J. K.; Ravikumar, G. Evaluation of Activation Energy and Thermodynamic Properties of Enzyme-Catalysed Transesterification Reactions. *Adv. Chm. Engineer. Sci.* 2012, *02* (01), 150–154. https://doi.org/10.4236/aces.2012.21018.

(22) Patil, P. D.; Gude, V. G.; Reddy, H. K.; Muppaneni, T.; Deng, S. Biodiesel Production from Waste Cooking Oil Using Sulfuric Acid and Microwave Irradiation Processes. *J. Environ. Prot.* 2012, *03* (01), 107–113. https://doi.org/10.4236/jep.2012.31013.

(23) Hannon, M.; Gimpel, J.; Tran, M.; Rasala, B.; Mayfield, S. Biofuels from Algae: Challenges and Potential; 2010.

(24) Demirbas Ayhan. A Realistic Fuel Alternative for Diesel Engines. *Springer: London* 2008, 213.

(25) Aboim Joseline Barbosa; Oliveira Deborah; Ferreira John Eric; Siqueira Andrei Santos; Dall'Agnol Leonardo Teixeira; Filho Geraldo Narciso Rocha; Gonçalves Evonnildo; Nascimento Luis Adriano. A Determination of Biodiesel Properties Based on a Fatty Acid Profile of Eight Amazon Cyanobacterial Strains Grown in Two Different Culture Media. *RSC Adv.* 2016, *6* (111), 109751-−109758.

(26) Osmont, A.; Catoire, L.; Gökalp, I.; Swihart, M. T. Thermochemistry of C - C and C - H Bond Breaking in Fatty Acid Methyl Esters. *Energy and Fuels* 2007, *21* (4), 2027–2032. https://doi.org/10.1021/ef070132e.

(27) Huynh, L. K.; Violi, A. Thermal Decomposition of Methyl Butanoate: Ab Initio Study of a Biodiesel Fuel Surrogate. *J. Org. Chm.* 2008, *73* (1), 94–101. https://doi.org/10.1021/jo701824n.

(28) Naik, C. V; Westbrook, C. K.; Herbinet, O.; Pitz, W. J.; Mehl, M.; Naik, C.; Westbrook, C.; Herbinet, O.; Pitz, W.; Mehl, M. Detailed Chemical Kinetic Reaction Mechanism for Biodiesel Components Methyl Stearate and Methyl Oleate. *Proc. Combust. Inst.* 2011, *33*, 383–389. https://doi.org/10.1016/j.proci.2010.05.007ï.

(29) Zhang, Y.; Dubé, M. A.; McLean, D. D.; Kates, M. Biodiesel Production from Waste Cooking Oil: 2. Economic Assessment and Sensitivity Analysis. *Bioresour. Technol.* 2003, *90* (3), 229–240. https://doi.org/10.1016/S0960-8524(03)00150-0.

(30) Zhang, Y.; Dubé, M. A.; McLean, D. D.; Kates, M. Biodiesel Production from Waste Cooking Oil: 1. Process Design and Technological Assessment. *Bioresource. Technol.* 2003, *90* (3), 229-240. https://doi.org/10.1016/S0960-8524(03)00040-3.

(31) Mizik, T.; Gyarmati, G. Economic and Sustainability of Biodiesel Production—A Systematic Literature Review. *Clean Technologies*. 2021, *3* (1), 19–36. https://doi.org/10.3390/cleantechnol3010002.

(32) Koh, M. Y.; Tinia, T. I. A Review of Biodiesel Production from Jatropha Curcas L. Oil. *Renew. Sust. Energ. Rev*. 2011, *15* (5), 2240–2251. https://doi.org/10.1016/j.rser.2011.02.013.

(33) U.S. Energy Information Administration. Total Energy. *Department of Energy*. https://www.eia.gov/totalenergy/data/monthly/ (accessed 2023-04-23).

(34) Hu, X.; Imran, M.; Wu, M.; Moon, H. C.; Liu, X. Alternative to Oil and Gas: Review of Economic Benefits and Potential of Wind Power in Pakistan. *Math. Probl. Eng*. 2020. https://doi.org/10.1155/2020/8884228.

(35) Demirtas, O. Evaluating the Best Renewable Energy Technology for Sustainable Energy Planning. *Int. J. Energy Econ. and Policy* 2013, *3*, 23–33.

(36) Wang, J. J.; Jing, Y. Y.; Zhang, C. F.; Zhao, J. H. Review on Multi-Criteria Decision Analysis Aid in Sustainable Energy Decision-Making. *Renew. Sust. Energ. Rev*. 2009, *13* (9), 2263–2278. https://doi.org/10.1016/j.rser.2009.06.021.

(37) Bakker Michael. Improving Biodiesel through Pyrolysis: Direct Dynamics Investigations Into Thermal Decomposition of Methyl Lineolate. MSc. Thesis Missouri State University, Springfield, MO, USA, 2020.

(38) Zou, C.; Zhao, Q.; Zhang, G.; Xiong, B. Energy Revolution: From a Fossil Energy Era to a New Energy Era. *Nat. Gas Ind.* 2016, *3* (1), 1–11. https://doi.org/10.1016/j.ngib.2016.02.001.

(39) Gervet, B.; Nordell, B. The Use Of Crude Oil In Plastic Making Contributes To Global Warming; 2007. https://www.researchgate.net/publication/266469821.

(40) Yang, F.; Hanna, M. A.; Sun, R. Value-Added Uses for Crude Glycerol--a Byproduct of Biodiesel Production. *Biotechnol. Biofuels* 2012, *5* (1). https://doi.org/10.1186/1754-6834-5-13.

(41) Demirbas, A.; Bamufleh, H. S. Optimization of Crude Oil Refining Products to Valuable Fuel Blends. *Pet. Sci. Tech.* 2017, *35* (4), 406–412. https://doi.org/10.1080/10916466.2016.1261162.

(42) Boris Brigljevic; Jay Liu. Process Design and Simulation of Industrial Scale Biofuel Production via Pyrolysis of Saccharina Japonica. *Adv. Control Ind. Process.* 2017.

(43) Fagan Marie N. Resource Depletion and Technical Change: Effects on U.S. Crude Oil Finding Costs from 1977 to 1994. *Energy Journal* 1997, *18*, 91–105.

(44) Augustine, C.; Tester, J. W.; Anderson, B.; Petty, S.; Livesay, B. A Comparison of Geothermal With Oil And Gas Well Drilling Costs.2016. https://www.academia.edu/17455693/A_Comparison_of_Geothermal_with_Oil_and_Gas Well_Drilling_Costs

(45) Xuechun, W.; Jianhua, F.; Boshui, C.; Jiu, W.; Jiang, W. Pyrolysis Characteristics and Kinetics of Methyl Oleate Based on TG-FTIR Method (1). *China Pet. Process. Petrochem. Technol.* 2015, *17* (2), 17–25.

(46) De Jong, S.; Hoefnagels, R.; Wetterlund, E.; Pettersson, K.; Faaij, A.; Junginger, M. Cost Optimization of Biofuel Production – The Impact of Scale, Integration, Transport and

Supply Chain Configurations. *Applied Energy* 2017, *195*, 1055–1070. https://doi.org/10.1016/j.apenergy.2017.03.109.

(47) Diévart, P.; Dooley, S.; Won, S. H.; Dryer, F. L.; Ju, Y.; Carter, E. A.; Law, C. K.; Green, W. H.; Hanson, R. K.; Davidson, D.; Hansen, N.; Klippenstein, S. J.; Sung, C.-J.; Egolfpoulos, F.; Wang, H. Development of Kinetic Models for Biodiesel Combustion. *Flame* 2010, *157* (6), 1116-1127

(48) Fukuda, H.; Kond0, A.; Noda, H. Review Biodiesel Fuel Production By Transesterification Of Oils. *J. Biosci. Bioeng.* 2001, *92* (5), 405-416.

(49) Balamurugan, S.; Seenivasan, D.; Rai, R.; Agrawal, A. Optimization of Biodiesel Production Process for Mixed Nonedible Oil (Processed Dairy Waste, Mahua Oil, and Castor Oil) Using Response Surface Methodology. *J. Process. Mech. Engin.* 2022, 1–13. https://doi.org/10.1177/09544089221147392.

(50) Mishra, S.; Anand, K.; Mehta, P. S. Predicting the Cetane Number of Biodiesel Fuels from Their Fatty Acid Methyl Ester Composition. *Energy and Fuels* 2016, *30* (12), 10425–10434. https://doi.org/10.1021/acs.energyfuels.6b01343.

(51) Sarathy, S. M.; Gaïl, S.; Syed, S. A.; Thomson, M. J.; Dagaut, P. A Comparison of Saturated and Unsaturated C4 Fatty Acid Methyl Esters in an Opposed Flow Diffusion Flame and a Jet Stirred Reactor. *Proc. Combust. Inst.* 2007, *31 I* (1), 1015–1022. https://doi.org/10.1016/j.proci.2006.07.019.

(52) Sui, M.; Li, F.; Wang, S.; Wang, H. Molecular Dynamics Simulation and Experimental Research on the Oxidation Reaction of Methyl Linoleate at Low Oxygen and High Temperature. *Fuel* 2021, *305*. https://doi.org/10.1016/j.fuel.2021.121478.

(53) Selvan, T.; Nagarajan, G. Combustion and Emission Characteristics of a Diesel Engine Fuelled with Biodiesel Having Varying Saturated Fatty Acid Composition. *Int. J. Green Energy* 2013, *10* (9), 952–965. https://doi.org/10.1080/15435075.2012.732157.

(54) Jiaqiang, E.; Liu, T.; Yang, W. M.; Li, J.; Gong, J.; Deng, Y. Effects of Fatty Acid Methyl Esters Proportion on Combustion and Emission Characteristics of a Biodiesel Fueled Diesel Engine. *Energy Convers. Manag.* 2016, *117*, 410–419. https://doi.org/10.1016/j.enconman.2016.03.021.

(55) Ozsezen, A. N.; Canakci, M. Determination of Performance and Combustion Characteristics of a Diesel Engine Fueled with Canola and Waste Palm Oil Methyl Esters. *Energy Convers. Manag.* 2011, 52, 108–116. https://doi.org/10.1016/j.enconman.2010.06.049.

(56) Saggese, C.; Frassoldati, A.; Cuoci, A.; Faravelli, T.; Ranzi, E. A Lumped Approach to the Kinetic Modeling of Pyrolysis and Combustion of Biodiesel Fuels. *Proc. Combust. Inst.* 2013, *34* (1), 427–434. https://doi.org/10.1016/j.proci.2012.05.020.

(57) Coniglio, L.; Bennadji, H.; Glaude, P. A.; Herbinet, O.; Billaud, F. Combustion Chemical Kinetics of Biodiesel and Related Compounds (Methyl and Ethyl Esters): Experiments and Modeling-Advances and Future Refinements. *Prog. Energy Combust. Sci.* 2013, *39* (4) 340–382. https://doi.org/10.1016/j.pecs.2013.03.002.

(58) Singh, G.; Jeyaseelan, C.; Bandyopadhyay, K. K.; Paul, D. Comparative Analysis of Biodiesel Produced by Acidic Transesterification of Lipid Extracted from Oleaginous Yeast Rhodosporidium Toruloides. *Biotech.* 2018, *8* (10). https://doi.org/10.1007/s13205-018-1467-9.

(59) Jahirul, M. I.; Rasul, M. G.; Chowdhury, A. A.; Ashwath, N. Biofuels Production through Biomass Pyrolysis- A Technological Review. *Energies*. 2012, *5* (12), 4952–5001. https://doi.org/10.3390/en5124952.

(60) Mao, X.; Xie, Q.; Duan, Y.; Yu, S.; Nie, Y. Pyrolysis of Methyl Ricinoleate: Distribution and Characteristics of Fast and Slow Pyrolysis Products. *Materials* 2022, *15* (4). https://doi.org/10.3390/ma15041565.

(61) Irawan, B.; Rusdianasari; Hasan, A. Pyrolysis Process of Fatty Acid Methyl Ester (FAME) Conversion into Biodiesel. *Int. J. Res. Vocat. Stud. (IJRVOCAS)* 2021, *1* (2), 01–10. https://doi.org/10.53893/ijrvocas.v1i2.21.

(62) Wang Xuechun; Fang Jianhua; Chen Boshui; Wang Jiu; Wu Jiang. Pyrolysis Characteristics and Kinetics of Methyl Oleate Based on TG-FTIR Method. *China Pet. Process. Petrochem. Technol.* 2015, *17* (2), 7-25.

(63) Koch, W.; Holthausen, M. C. A Chemist's Guide to Density Functional Theory. 2nd ed.; Wiley-VCH Verlag GmbH: Weinheim, Germany 2001. ISBNs: 3-527-6004-3

(64) Kurth, S.; Marques, M. A. L.; Gross, E. K. U. *Electronic Structure: Density Functional Theory*. Institut für Theoretische Physik, Freie Universität Berlin, Arnimallee 14, D-14195 Berlin, Germany 2003. PACS numbers: 71.15.Mb, 31.15.Ew.

(65) Bagayoko, D. Understanding Density Functional Theory (DFT) and Completing It in Practice. *AIP Advances* 2014, *4* (12). https://doi.org/10.1063/1.4903408.

(66) Prasad, V. K.; Otero-De-La-Roza, A.; Dilabio, G. A. Small-Basis Set Density-Functional Theory Methods Corrected with Atom-Centered Potentials. *J. Chem. Theory Comput.* 2022. *18*, 2913-2930. https://doi.org/10.1021/acs.jctc.2c00036.

(67) Amber, S.; Kamal, M. A. Production of Hydrocarbons by Catalytic Cracking of Stearic Acid under Atmospheric Pressure for Petrochemical Replacement. *Pet. Sci. Technol.* 2019, *37* (2), 146–154. https://doi.org/10.1080/10916466.2018.1522334.

(68) Baseden, K. A.; Tye, J. W. Introduction to Density Functional Theory: Calculations by Hand on the Helium Atom. *J. Chem. Edu.* 2014, *91* (12), 2116–2123. https://doi.org/10.1021/ed5004788.

(69) Liu, J.; Guo, X. ReaxFF Molecular Dynamics Simulation of Pyrolysis and Combustion of Pyridine. *Fuel Process. Technol.* 2017, *161*, 107–115. https://doi.org/10.1016/j.fuproc.2017.03.016.

(70) Guo, X.; Liu, Z.; Liu, Q.; Shi, L. Modeling of Kraft Lignin Pyrolysis Based on Bond Dissociation and Fragments Coupling. *Fuel Process. Technol.* 2015, *135*, 133–149. https://doi.org/10.1016/j.fuproc.2014.12.009.

(71) Jambrina, P. G.; Aldegunde, J. Computational Tools for the Study of Biomolecules. *Comput. Aided Chem. Eng.* 2016. *39*, 583–648. https://doi.org/10.1016/B978-0-444-63683-6.00020-4.

(72) Bhoi, S.; Banerjee, T.; Mohanty, K. Molecular Dynamic Simulation of Spontaneous Combustion and Pyrolysis of Brown Coal Using ReaxFF. *Fuel* 2014, *136*, 326–333. https://doi.org/10.1016/j.fuel.2014.07.058.

(73) Van Gunsteren, W. E.; Berendsen, H. J. C. Computer Simulation of Molecular Dynamics: Methodology, Applications, and Perspectives in Chemical reviews. *Angew. Chem. Int. Ed. Engl.* 1990. *29*, 992-1023.

(74) Pires de Oliveira, I.; Caires, A. R. L. Molecular Arrangement in Diesel/Biodiesel Blends: A Molecular Dynamics Simulation Analysis. *Renew. Energy* 2019, *140*, 203–211. https://doi.org/10.1016/j.renene.2019.03.061.

(75) Bircher, M. P.; López-Tarifa, P.; Rothlisberger, U. Shedding Light on the Basis Set Dependence of the Minnesota Functionals: Differences between Plane Waves, Slater Functions, and Gaussians. *J. Chem. Theory Comput.* 2019, *15* (1), 557–571. https://doi.org/10.1021/acs.jctc.8b00897.

(76) Wannarumon, S.; Grande, M. A. Comparisons of Computer Fluid Dynamic Software Programs Applied to Jewelry Investment Casting Process. *World Acad. Sci. Eng. Technol.* 2009, *55*, 88–95.

(77) Walker, M.; Harvey, A. J. A.; Sen, A.; Dessent, C. E. H. Performance of M06, M06-2X, and M06-HF Density Functionals for Conformationally Flexible Anionic Clusters: M06 Functionals Perform Better than B3LYP for a Model System with Dispersion and Ionic Hydrogen-Bonding Interactions. *J. of Phys. Chem. A* 2013, *117* (47), 12590–12600. https://doi.org/10.1021/jp408166m.

(78) Zhao, Y.; Truhlar, D. G. The M06 Suite of Density Functionals for Main Group Thermochemistry, Thermochemical Kinetics, Noncovalent Interactions, Excited States, and Transition Elements: Two New Functionals and Systematic Testing of Four M06-

Class Functionals and 12 Other Functionals. *Theo. Chem. Acc.* 2008, *120* (1–3), 215–241. https://doi.org/10.1007/s00214-007-0310-x.

(79) Mcleod, S. What Are Confidence Intervals in Statistics*?*.2019. https://www.simplypsychology.org/statistics.html.

(80) Confidence Interval; 2022. https://en.m.wikipedia.org/wiki/Confidence_interval#.

(81) Glen, S. Z Alpha/2 (za/2): What it is, How to Find it. From StatisticsHowTo.com. https://www.statisticshowto.com/probability-and-statistics/find-critical-values/z-alpha2-za2/

(82) Chai Ming. Thermal Decomposition of Methyl Esters in Biodiesel Fuel: Kinetics, Mechanisms and Products, Ph.D. Thesis, University of Illinois at Urbana-Champaign, IL, USA, 2012.

(83) St. John, P. C.; Guan, Y.; Kim, Y.; Kim, S.; Paton, R. S. Prediction of Organic Homolytic Bond Dissociation Enthalpies at near Chemical Accuracy with Sub-Second Computational Cost. *Nat. Commun.* 2020, *11* (1). https://doi.org/10.1038/s41467-020-16201-z.